ANL-80-115
Part IV



ANL-80-115
Part IV



# RADIOLOGICAL AND ENVIRONMENTAL RESEARCH DIVISION ANNUAL REPORT

## Atmospheric Physics

## January—December 1980


ARGONNE NATIONAL LABORATORY, ARGONNE, ILLINOIS

Prepared for the U. S. DEPARTMENT OF ENERGY
under Contract W-31-109-Eng-38

Distribution Category:
Environmental Control Technology
and Earth Sciences (UC-11)

ANL-80-115
Part IV

ARGONNE NATIONAL LABORATORY
9700 South Cass Avenue
Argonne, Illinois 60439

# RADIOLOGICAL AND ENVIRONMENTAL RESEARCH DIVISION ANNUAL REPORT

## Atmospheric Physics

January--December 1980

R. E. Rowland, Division Director
B. B. Hicks, Section Head

August 1981



**Preceding Report: ANL-79-65, Part IV, January--December 1979**

## FOREWORD

The Atmospheric Physics Section continues to concentrate research activities on the transport, removal and, to a lesser extent, transformation of pollutants in the lower atmosphere. Concerning transport, techniques of remote sensing are being developed further and, as reported here, have been applied to examine flow patterns in the mountainous terrain of the Geysers Area in Northern California, as part of the Atmospheric Studies of COmplex Terrain (ASCOT) of DOE. Our effort for ASCOT also utilizes numerical models to consolidate and interpret the experimental information and to extend the results to flow above different types of nonhomogeneous surfaces. In related studies for DOE, land and lake (or sea) breezes that tend to confine pollutants in partially closed circulations are being investigated. Nevertheless, as it has in the past, study of flow over nearly uniform terrain plays an important role. For example, one phase of the work for the Multistate Atmospheric Power Production Pollution Study (MAP3S) of EPA is on the enhanced low-level nocturnal horizontal advection of pollutants over flat terrain during very stable conditions.

Study of the various physical processes that control atmospheric concentrations of pollutants emitted from diesel engines in urban areas is an ongoing research effort. Arising from a multilaboratory DOE program, this work centers on wind-tunnel simulations, field experiments, and theoretical investigations, all directed towards developing better parameterizations of flow patterns in street canyons, surface deposition, and particle physics. Concurrently, numerical simulations that use the parameterizations are being developed and applied.

The air-surface exchange of trace materials in the atmosphere continues to be studied experimentally, by use of previously-developed micrometeorological techniques, and theoretically, as is necessary to interpret resulting field data of a type rarely, if ever, gathered before. Two EPA programs, one of them MAP3S, support this work, while the DOE-supported effort is primarily devoted to the air-water exchange of pollutants. A related research project, just begun in 1980, concerns the air-sea exchange of carbon dioxide and is part of the ongoing Carbon Dioxide and Climate Research Program of DOE. As a result of our involvement in this

program, there is some preliminary work being done on examining short-term climate trends possibly evident in meteorological data gathered routinely by this Section.

A major effort for MAP3S and related programs has been on numerical simulations of the regional-scale behavior of pollutants important in determining the acidity of precipitation. The Advanced Statistical Trajectory Regional Air Pollution (ASTRAP) model has proven an effective means, for example, to estimate the flux of sulfur pollutants across the border between Canada and the United States, and thus produces results that are being examined in the establishment of international legal agreements. The ASTRAP model relies heavily on parameterizations developed and being improved by this Section as a result of experimental and theoretical work. A recent addition to this effort has been the modeling of chemical transformation processes in the lower atmosphere.

As a result of the current emphasis on "acid rain," precipitation at the Argonne site has been collected and analyzed extensively. Our first efforts are centered on understanding the sampling and analysis errors that might have led to misconceptions on the severity and extent of acid rain in the past. This work, as part of the multilaboratory studies supported by MAP3S/EPA and DOE, is directed toward developing better parameterizations of precipitation scavenging of atmospheric pollutants, for use in numerical models such as ASTRAP that compute regional-scale deposition.

This document summarizes work by this Section in a manner similar to the most recent Annual Reports. A sampling is given rather than a full representation of all work performed and the articles are short progress reports rather than full accounts. Clearly, some of the findings reported are preliminary or are intermediate steps leading to application of techniques. Readers should seek the open-literature publications in order to study the completed phases of the work in detail.

TABLE OF CONTENTS

# SODAR INVESTIGATIONS IN COMPLEX TERRAIN

R. L. Coulter

The ASCOT (Atmospheric Studies in COmplex Terrain) 1980 experiment took place in Anderson Creek Valley in Northern California. Part of this Section's involvement was operation of the ANL Doppler sodar to evaluate the wind field between 50 and 500 m, and to delineate atmospheric structure through the amplitude of the returned signals. The sodar was located at the Television Repeater site (TVR), approximately 2 km northwest of and 100 m above the outflow region of the valley (Coulter, 1980, Fig 1). This location can be influenced by drainage flow from Anderson Creek to the west, Putah Creek to the north and, on rare occasions, Bear Creek to the south. The surrounding ridges of the valley are about 500 m above the TVR site.

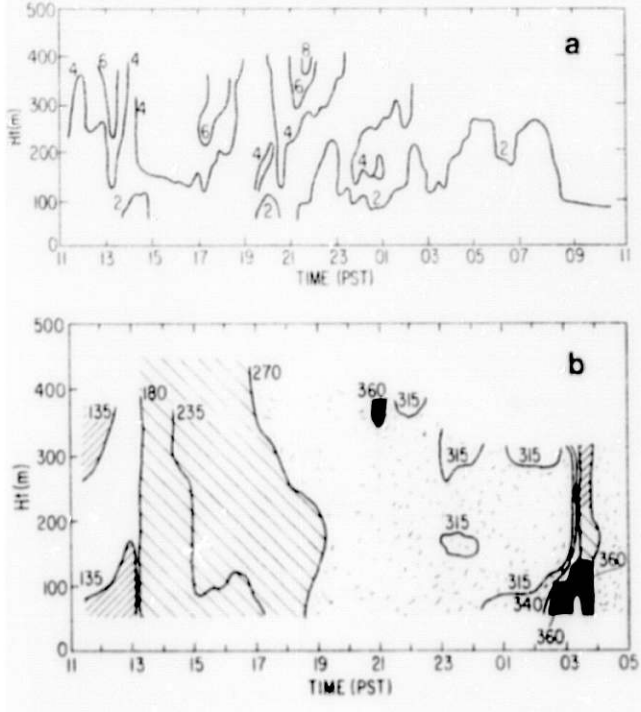


FIG. 1. Wind speed (a) and direction (b) contours from sodar data.

During the experimental period, September 9 through September 25, five nights were selected for full-scale nocturnal drainage experiments, which included tracer releases, tethered balloon soundings, laser anemometer operations, radon sampling, and tracer collection at a multitude of sites throughout the valley. The ANL sodar operates semi-continuously in various modes throughout the period. This report discusses only the horizontal wind circulations observed during the period.

Figure 1 shows a typical diurnal cycle of observed wind speed and direction. Light wind conditions were prevalent throughout the period. Morning and early afternoon easterly winds associated with convective, upslope flow were replaced in mid-afternoon by stronger southwesterly winds, most

likely associated with a sea breeze from the Pacific Ocean, approximately 65 km to the southwest. Because of the cold Pacific water temperatures near

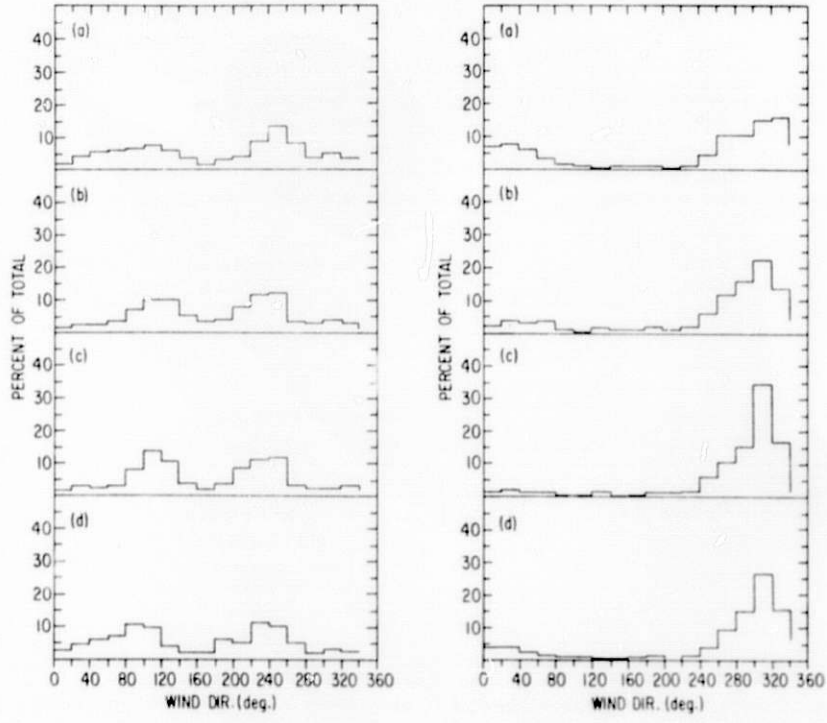


FIG. 2. Histogram of wind directions during nighttime (left) and daytime (right) hours at 100 m increments (a-d) on five experimental days during September, 1980.

northern California, the temperature difference between land and sea was still quite large, even in late September.

During the early evening hours (1800-2000) the winds shifted to the west or northwest, oriented along Anderson Valley. Throughout the evening this alignment was occasionally contested both from below and from above. The larger scale, synoptically driven flow sometimes intruded from above into the high levels; the height to which these flow patterns descended probably depended upon their strength and the stability of the drainage flow regime. For example, note the easterly flow above 150 m from midnight until 0200, with duration of the intrusion increasing with height. Also in the evening hours, a "contest" was waged between the Anderson Valley (NW) and Putah (NNE). Note the occasional transitions to NE flow in the lowest level. The TVR site is nominally within Anderson Valley, but located on a side slope barely removed from the side of Putah, a narrower, more precipitous (at this location) valley.

Finally, with sunrise, a transition took place between drainage flow and upslope flow created by heating of the sides of the valley. Perusal of the data, however, reveals that, particularly in the lowest layers, the wind direction shifted first to the NE rather than E. Presumably the drainage flow in Putah Creek did not cease as early as that in Anderson because the high N-S ridge blocked the direct solar heating. Thus the Putah Creek drainage flow at TVR probably replaced the rising air created by surface heating more efficiently than return flow up Anderson Valley. Later in the morning, with heating in Putah Valley, the flow at TVR became easterly, corresponding to upslope flow in Anderson Valley.

Figure 2 illustrates the predominant flow regimes partitioned by daytime and nighttime hours. Further inspection of non-experimental days shows smaller differences in daytime vs. nighttime periods due to stronger synoptic forcing, which leads to a slightly more uniform histogram of wind directions in non-experimental conditions.

Wind speeds throughout were quite light, generally less than 8 m $s^{-1}$. While nocturnal "jets" are common in flat, homogeneous terrain (see Coulter, 1980), the nocturnal wind profile showed only a very weak and occasional jet. This is not at all surprising, since the terrain is extremely inhomogeneous as well as sloping; the effects of the drag due to the surface are not greatly reduced with cessation of surface heating.

## Reference

Coulter, R. L., 1980: Nocturnal low-level wind maxima at Argonne, this report.

LASER ANEMOMETER RESULTS FROM ASCOT 1980

R. L. Coulter and T. J. Martin

The ASCOT (Atmospheric Studies in COmplex Terrain) 1980 experiment in the Geysers area of northern California was an investigation into the characteristics of nocturnal drainage flow in complex terrain. The field study took place in Anderson Creek valley (oriented roughly E-W, see Figure 1), which in turn has three additional creeks and associated valleys draining into it: Putah Creek from the north, Bear Creek from the south, and Gunning Creek from the northwest. Add to this the small scale terrain variations within the valley itself and one has a multitude of possible variations in the flow. As part of this Section's experimental efforts during September 1980, three laser anemometers were operated roughly perpendicular to expected drainage flows to measure line-averaged values of wind speed.

The Davies site, located at the mouth of the valley, was within a relatively narrow channel. The Jenkins site was located about 4 km WNW, some 200 m above the Davies site. The Bianchi site was also 4 km WNW of Davies but oriented roughly perpendicular to and about 100 m above Jenkins (see Figure 1). The Davies path averaged 23 m above the ground over its 600 m length.

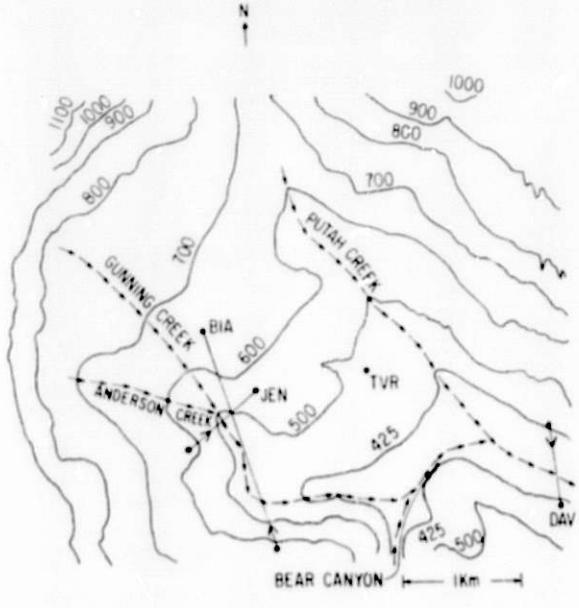


**FIG. 1. Topographical map of experimental area. Davies (DAV), Jenkins (JEN), and Bianchi (BIA) laser paths are indicated.**

The Jenkins path, complicated by a 60 m height difference between endpoints over a steeply cut descent to Anderson Creek, averaged 59 m above the surface through an 860 m path. The Bianchi path was relatively long (1910 m) and averaged 98 m above the surface. Thus, the three samples provided very different aspects of the valley flow characteristics.

Figure 2 shows the wind speed perpendicular to the laser paths for a 24 hour period. There is a noticeable difference in the character of the

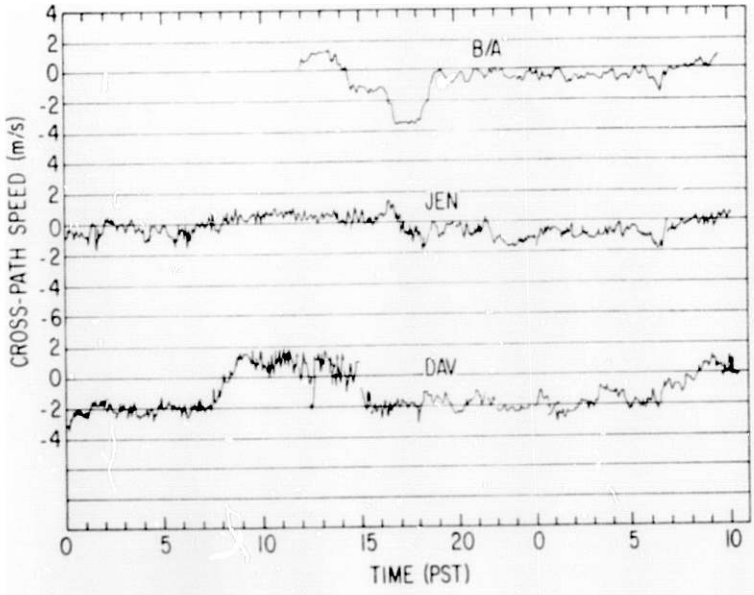


FIG. 2. Wind component measured at each of the three sites on September 16, 1980.

trace during the nocturnal periods, particularly at the Davies site. When flow becomes downslope the high frequency fluctuations decrease in amplitude, corresponding to the absence of strong thermal mixing. The Davies location evinces much greater downslope flow than the upper sites, even though the terrain is falling away much less rapidly. This is due to the constriction of flow at the Davies site as drainage from Anderson, Bear and Putah Creeks converges nearby. The transition to thermally-forced upslope flow during daytime is readily apparent at both Davies and Jenkins but somewhat less so at Bianchi. The influence of a possible sea breeze circulation can be seen at both Bianchi and Davies but not Jenkins, because of its orientation roughly perpendicular to a sea breeze front.

Spectra from each of the sites (Figure 3), averaged over four nights (between 1800 and 0600 hr the following day) indicate a common mode near 1.5 hr. Daytime spectra (not shown) for Jenkins and Bianchi have no such peak, although the daytime Davies spectrum does. Each of the three sites has a broad spectral peak for nocturnal periods near 30 min--somewhat shorter for Davies, somewhat longer for Bianchi (perhaps related to differences in their height above ground level). The Davies spectrum falls off much more than the other two at periods less than 15 min, quite probably because of greater domination by the drainage flow. Topographical influences in the spectra can be investigated by normalizing the spectra by the mean wind speed through the 12 hour period. When this is done, the Bianchi and Davies sites have similar

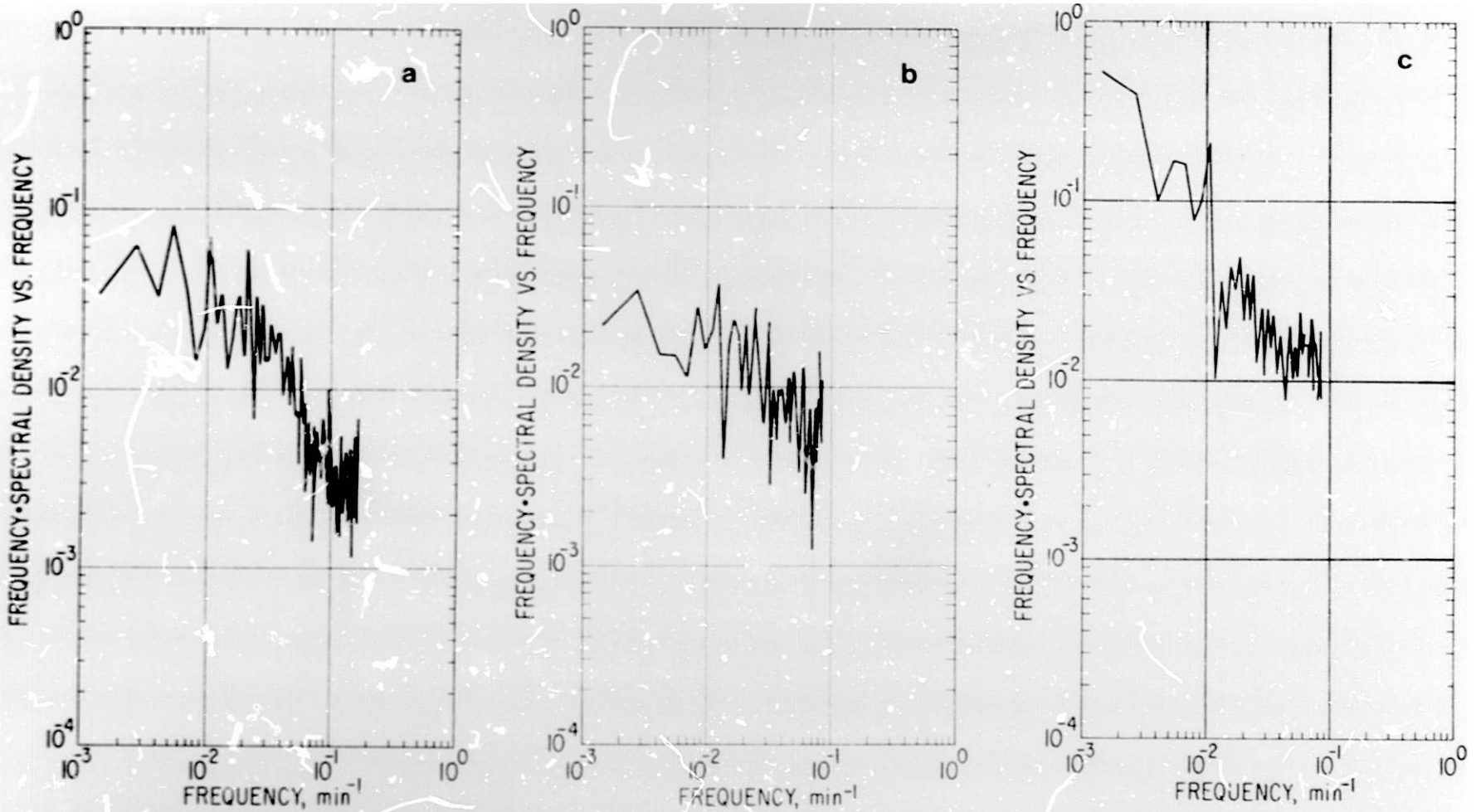


FIG. 3. Spectra of laser anemometer data from (a) Davies, (b) Jenkins, and (c) Bianchi sites averaged over four 12 hr experimental periods centered around midnight (beginning September 15, 18, 19, and 23).

peaks near 1 hr, which correspond to 1750 m for Bianchi and 5000 m for Davies. Jenkins exhibits no such peak.

# NOCTURNAL LOW-LEVEL WIND MAXIMA AT ARGONNE

R. L. Coulter

Proper simulation of long-range transport of pollutants requires characterization of the nocturnal planetary boundary layer. With cessation of surface heating and elimination of buoyancy as a source of turbulence near sunset, mixing in the lower atmosphere results from turbulence produced only by mechanical forces associated with wind shear. Following stable stratification due to surface cooling, winds aloft become less strongly coupled to the surface through frictional forces. The winds aloft accelerate and occasionally become larger than the geostrophic wind as a result of inertial oscillation (Blackadar, 1957). The resulting nocturnal low-level wind maximum or "jet" has the potential for greater horizontal pollutant transport than normally occurs during the daytime. This report describes an experimental investigation initiated at Argonne in July 1980 into the characteristics of wind profiles during nighttime hours.

Wind profiles are obtained with the Doppler sodar system developed in this Section. The sodar also provides data on the depth of the nocturnal inversion or, more strictly, on the depth of the mixing created by wind shear where strong temperature gradients exist. An instrumented tower at ANL provides additional wind data at 44 m (a height slightly below the lowest height accessible with sodar), the surface air temperature, and wind and temperature differences between 1.5 and 6 m.

Days with clear skies were chosen for most of the cases studies thus far--optimum conditions for the necessary rapid cooling and decoupling from the surface. Thus, statistics on the samples to date are not unbiased in terms of probability of jet occurrence. Figure 1 shows the development of the jet through one night. Note the good correlation between jet height and inversion depth. Even though the magnitude of this jet is small, wind speeds are elevated through approximately 100 m. Although a nocturnal jet occurs quite often (see Table 1), it rarely follows exactly the script written for it by classical theory, particularly at sites (such as ANL) that are not perfectly homogeneous in terrain and that can be affected by mesoscale meteorological features.

Table I. Summary of cases of nocturnal low level wind maxima for July 1980 - February 1981

| | |
|---|---|
| Number of cases | 25 |
| Number of jets longer than 2 hr | 21 |
| Number of jets longer than 6 hr | 15 |
| Number of jets longer than 10 hr | 6 |
| Number with maximum wind speed > 10 m/s at some time | 15 |
| Number with maximum wind speed > 15 m/s at some time | 8 |
| Number with maximum wind speed > 20 m/s at some time | 1 |
| Number with correlation of jet to inversion ht. > 0.0 | 15 |
| Number with correlation of jet to inversion ht. < 0.0 | 6 |
| Number where jet ht. changes its association from surface to elevated inversion | 5 |
| Number from above which have correlation < 0.0 | 4 |
| Average height of inversion (weighted by event) | 165 m |
| Average height of jet maximum (weighted by event) | 165 m |
| Correlation of nightly averages of inversion to jet height | 0.54 |
| Average height of inversion (weighted by duration) | 167 m |
| Average height of jet maximum (weighted by duration) | 160 m |
| Correlation of average inversion to jet height (weighted by duration) | 0.64 |
| Average standard deviation of inversion height | 56 m |
| Average standard deviation of jet maximum height | 0.38 |

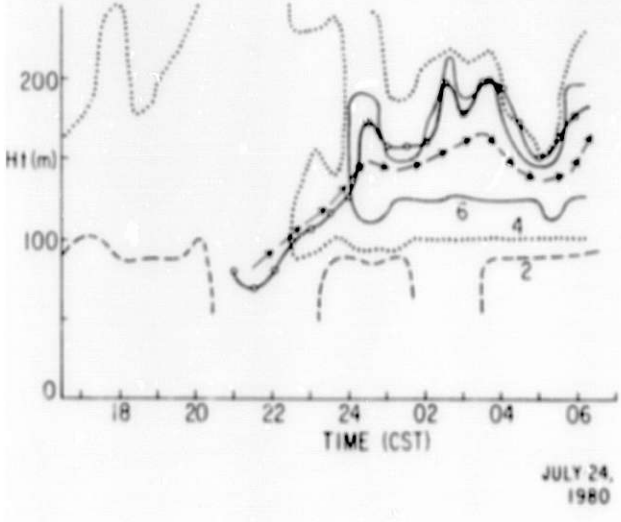


FIG. 1. Contours of wind speed through the night of August 5, 1980. Countours are in m $s^{-1}$. Open circles indicate the height of the surface inversion and arrows indicate the height of the wind maximum. Shaded area indicates portions th speeds above 6 m $s^{-1}$.

Table 1 lists the overall features of 25 cases studied through January, 1981. Some cases have been deleted from the original data set because of problems with echoes in low-level returns, a problem accentuated by refraction in stable conditions. Note the high rate of jet occurrence (84%) even through the late fall and early winter, a period not considered optimum for jet formation. A strong correlation is found between the height of the jet and the depth of the nocturnal inversion as determined by the sodar. The exact agreement of the average of the nightly inversion and jet heights must be regarded as coincidental, for on a night-by-night basis they certainly are not identical.

Because of the large variation in the quality of the data due to problems such as caused by echoes in lower layers and by the inability to detect jets at great heights, it is useful to limit the data set still further in order to study the details of jet development. The set can be limited to twelve cases by choosing jets of long duration and well defined maxima. Of these twelve cases, ten developed before midnight, four before 2000 hrs. Five cases found the height of the maximum wind speed increasing more than 50 m, four decreasing more than 50 m. In all twelve cases the jet height was very nearly in phase with the surface inversion height. Perhaps most interesting, however, is that in ten cases the beginning of the jet came about at the same time as, or just subsequent to, some perturbation in the surface inversion. Usually this was in the form of an elevated layer descending to and merging with the surface inversion. At that time, speeds at jet height increased by an average of 2 m/s within one averaging period; in two cases there was no acceleration, but the speeds above the height of the apparent wind maximum decreased markedly to form the jet.

The inclusion of data taken throughout spring and summer, 1981, should enhance the data set to the point that more definite conclusions about the formation, development and persistence of nocturnal wind maxima can be made.

## Reference

Blackadar, A., 1957: Boundary layer wind maxima and their significance for the growth of the nocturnal inversions, Bull. Am. Meteorol. Soc. 38(5).

# THREE-DIMENSIONAL SODAR CAPABILITIES

R. L. Coulter and T. J. Martin

During the past two years, this Section has been upgrading its capabilities in the remote sensing of the Planetary Boundary Layer (PBL), in particular through the development of a Doppler sodar capable of measuring turbulence parameters (temperature and velocity structure parameters) and the mean wind structure up to 1 km above the ground.

Designed around an LSI-11 microcomputer* and a Quan Tech Transponder and Clock and Timing generator, this system is very versatile. In order to determine the complete wind vector, three independent measurements of the wind speed are made. This is accomplished with three separated transmitters, one of which points vertically and also acts as the receiver for all three signals. Thus, only the vertically pointing transmitter-receiver need be acoustically shielded from ambient noise and, as a result of the vertical orientation of the transmitter-receiver, less ambient noise is incident upon the antenna. Separated from the receiver by as much as 300 m, the other two transmitters are large horns (1.6 m long, 1 m × 1 m opening) capable of an electrical output of 200 W. Thermostatically controlled transducer heaters allow for operation through freeze-thaw cycles in the presence of condensation.

Modifications to the clock and timing generator enable any or all of the transmitters to operate alternately. The rms-detected signal strength as well as the in-phase and quadrature-phase signals are provided by the transponder to the microcomputer, and a calculation of the signal-to-noise ratio (SNR) is provided by a small analog computer (developed in-house). If the SNR is above a threshold value the microcomputer calculates the Doppler shift of the signal through calculation of the complex covariance of the in-phase and quadrature-phase signals over the selected height interval. Because of the geometry involved, the number of samples per height interval is not constant; this is taken into account by the system. Only if consecutive

* This does not imply endorsement of this product over others capable of the same performance.

values from the two separated transmitters are above the SNR threshold is the horizontal wind calculated from these signals and corrected for any vertical velocity measured by the transmitter-receiver. These height-averaged values as well as the rms amplitude and wind direction (calculated from the horizontal measurements) are then averaged over a selected time interval and stored on a floppy disk. In addition, values of the standard deviation of the horizontal wind, vertical wind, and wind direction are stored. Finally, the number of times the SNR threshold was exceeded in each time interval (a measure of the reliability of the estimate) is stored for each average. A plot of the latest profile of horizontal wind, vertical wind, and wind direction is produced on a display terminal. If only vertical velocities are being monitored, a "map" of the magnitudes is produced on the terminal with more intense regions representing larger vertical velocities.

Several systems are available for pictorial displays of the signal amplitude (see Martin, 1980), some of which operate via microcomputer and an on-line printer and others through a completely independent small microprocessor and printing terminal.

In any given period of data collection with this system the following parameters may be changed at will:

1. SNR threshold
2. Number of pulses to average
3. Maximum height to acquire data
4. Height interval over which to average
5. Type of profile (three components or vertical only)
6. Baseline of separated transmitters (need not be the same)
7. Orientation of transmitters (except 0° or 180° relative to each other)
8. Relative height of transmitters and receivers
9. Elevation angle of transmitters

Constant parameters are:

1. Sampling rate (200 Hz)
2. Bandwidth (100 Hz)

The first four parameters can be changed during operation of the system and will take effect on the subsequent average. Under the present configuration, data can be taken continuously for approximately one week before storage is exhausted.

Reference

Martin, T. J., 1980: Sodar intensity display techniques, this report.

SODAR INTENSITY DISPLAY TECHNIQUES

T. J. Martin

Four inexpensive hard-copy gray-scale display techniques have been implemented and tested as a means of displaying sodar return signal strength. The first method, alphanumeric character plotting, is one of the simplest techniques for representing gray scale (Figure 1). Other than the ease of implementation, the primary advantage of this technique is that intensity level can be easily read and compared over various portions of the record. Overprinting is unnecessary for displaying the approximately eight gray levels that can be discerned by the eye, and is not desirable since it obscures individual character readability when intensity comparisons are made. The primary disadvantage of character plotting is that the large character size results in excessive use of paper when individual sodar pulses

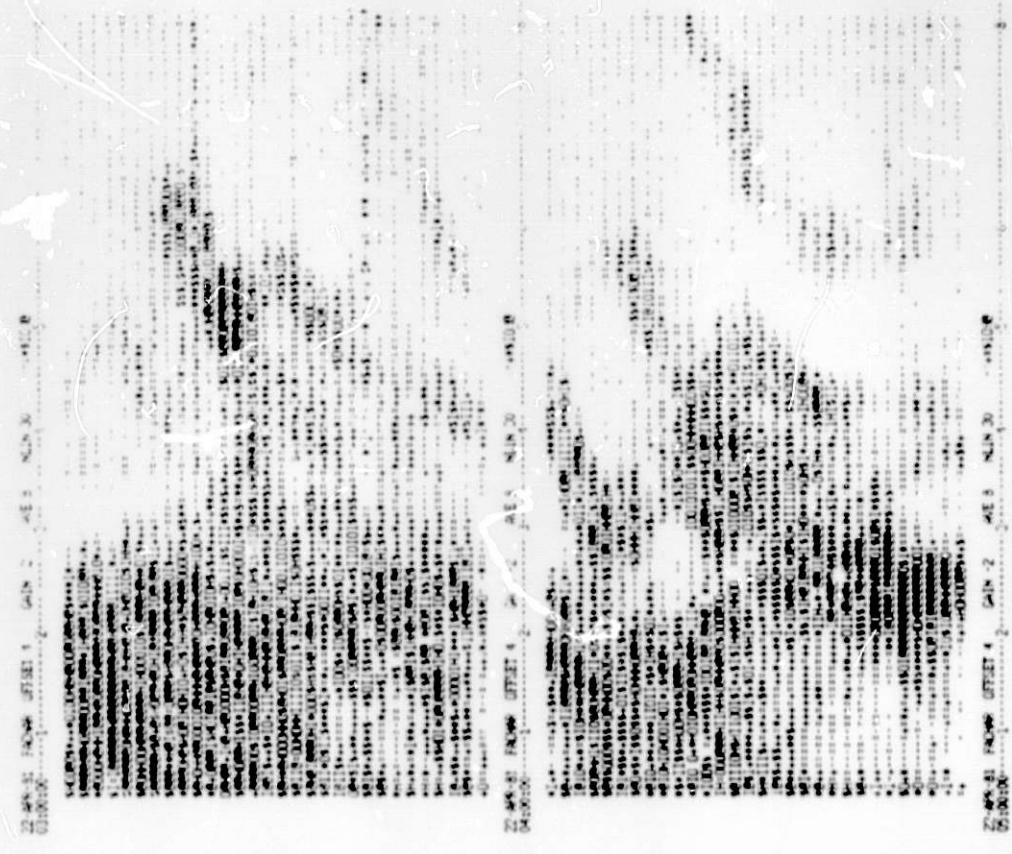

FIG. 1. Alphanumeric character plot of sodar return signal strength for an April day, 0200-0600 CST, 0 to 800 meters height.

are plotted. Signal averaging is required to keep paper use to reasonable levels for long-term data logging.

Information density can be increased and smoothness of the gray-scale record enhanced if a matrix of closely-spaced dots is used to represent gray levels. This requires a printer with graphics capabilities that allow for control of individual dots. We have chosen a 3 × 3 matrix of dots (pixel) to represent ten gray levels. Proper placement of dark dots within the pixel for the various gray levels is important in avoiding confusing patterns that can arise within a collection of pixels. The patterns we have selected are shown at the top of Figure 2. The pixel technique (bottom of Figure 2) is very good for producing a smooth and wide gray-scale dynamic range. The graphics printer used has a linear density of 70 dots per inch; as a result, the

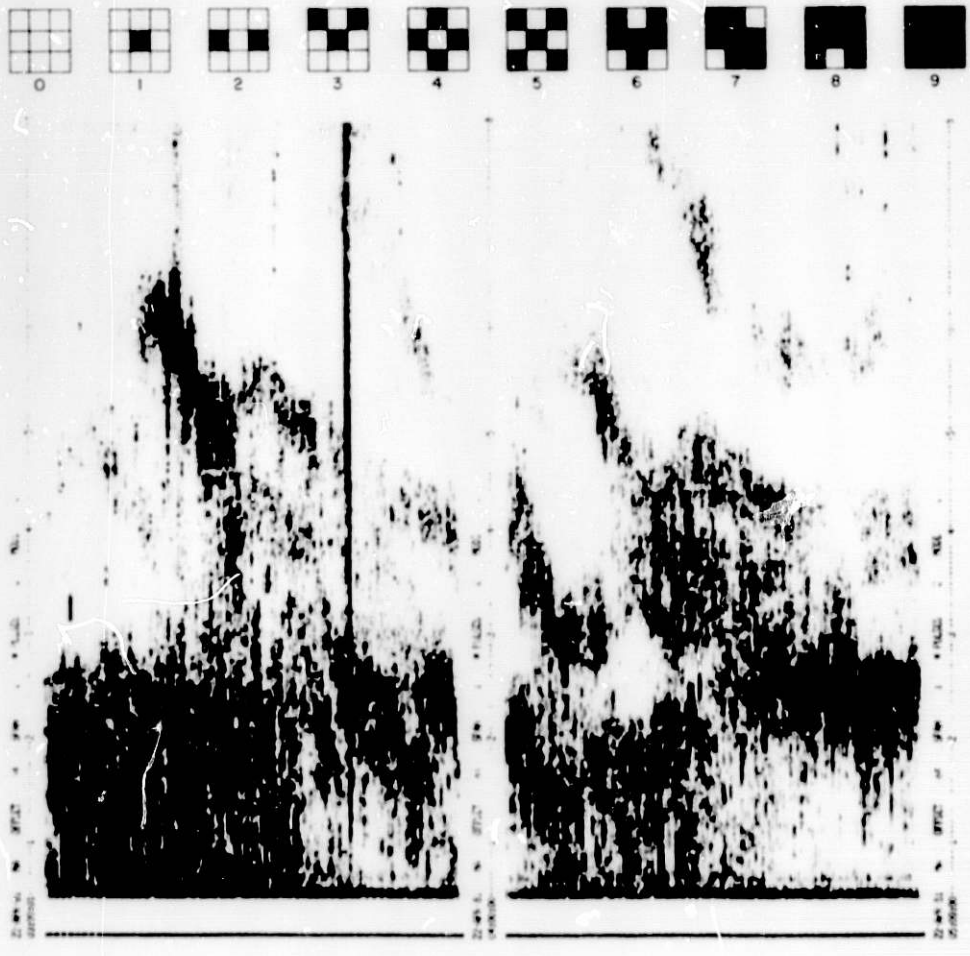


FIG. 2. (top) 3 × 3 pixel character set;
(bottom) 3 × 3 pixel plot as in Figure 1.

plotting of individual sounder returns still requires considerable amounts of paper.

In an effort to increase further the information density in gray-scale plotting so that individual sodar returns can be compactly plotted, we have used a random dot control technique (Figure 3). This method prints a dot only if the input intensity level is greater than a random number generated for comparison with each dot position. Thus, high intensity signals allow more dots to be printed than low intensity signals. For a properly scaled input, the number of gray levels is related to the number of random number levels. The resultant image is surprisingly good, although precise information about the intensity levels within sodar returns is lost. It may be useful to note that this technique could also be implemented quite easily with analog techniques using white noise, sample and hold, and comparator circuits.

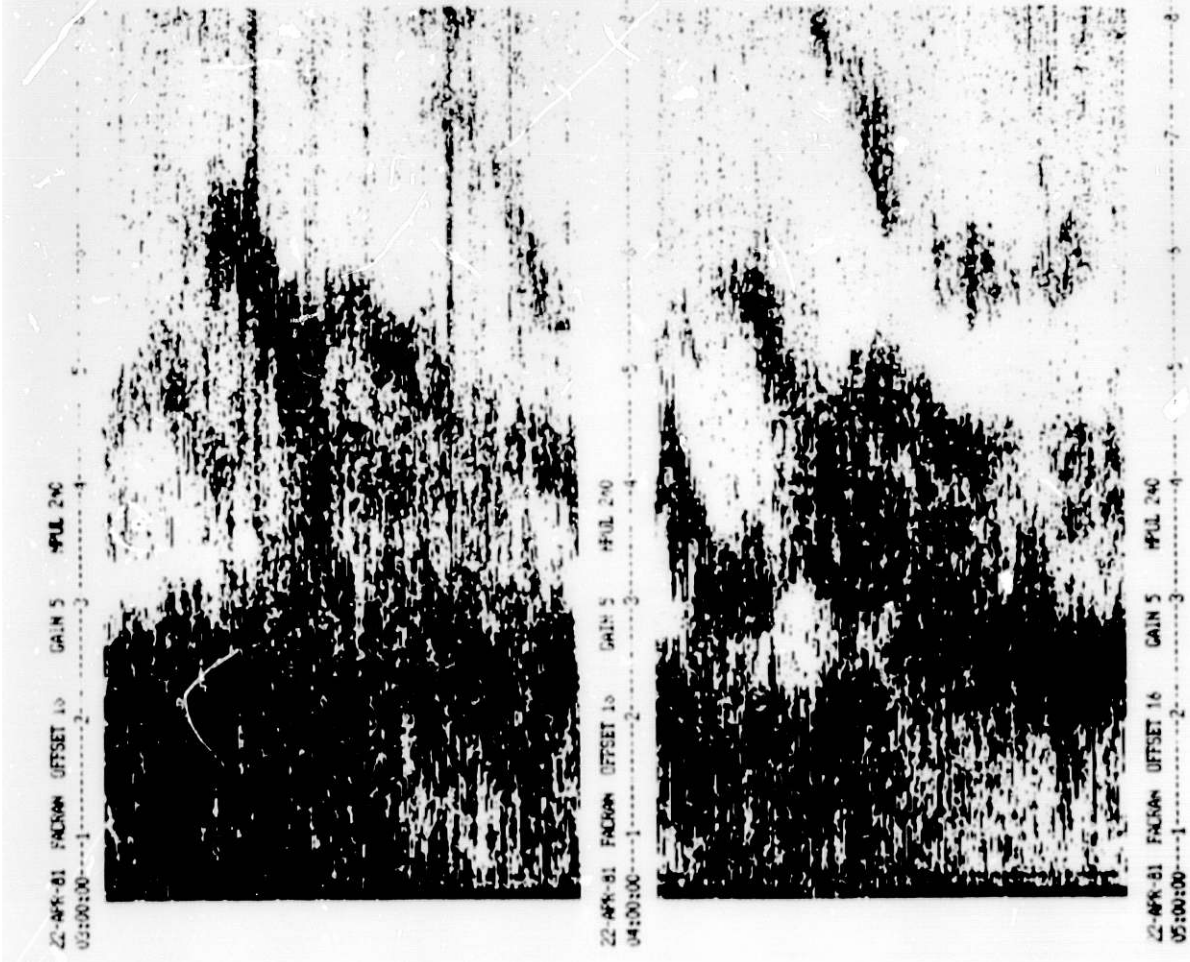


FIG. 3. Random dot control plot, as in Figure 1.

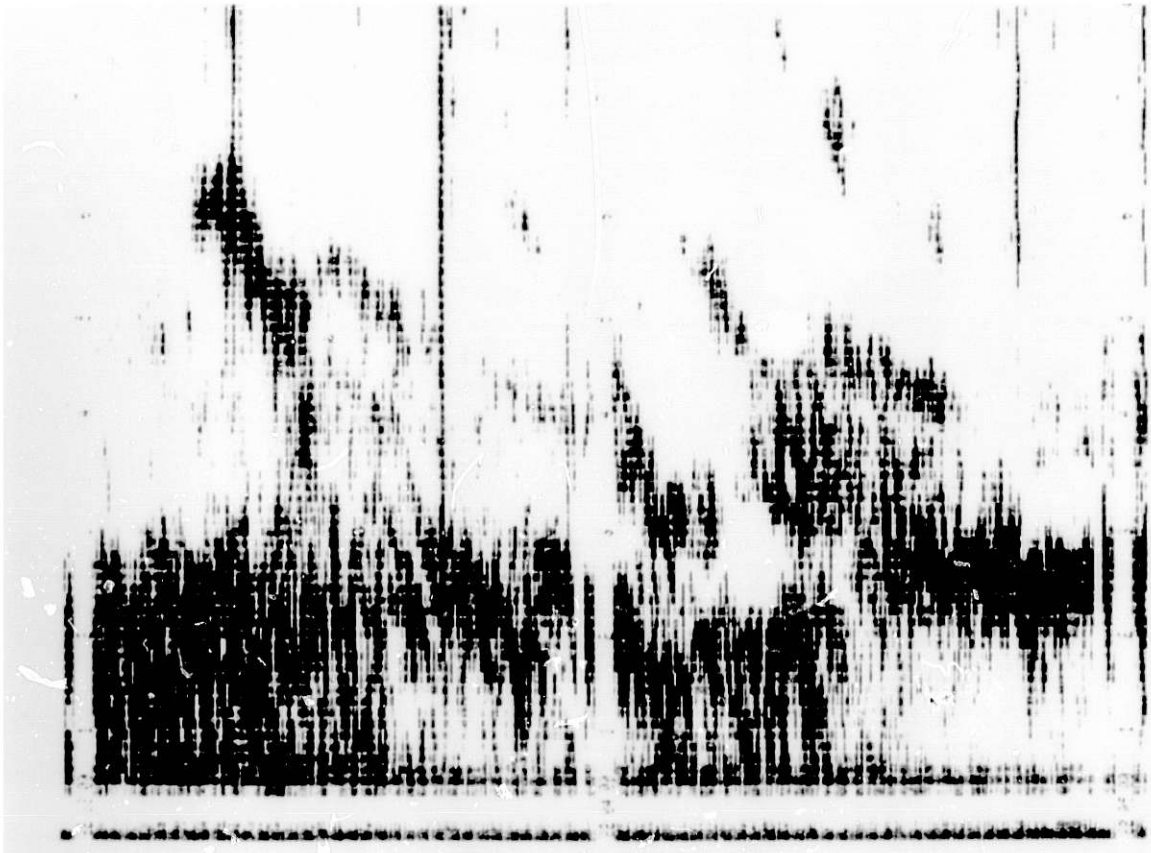

FIG. 4. Thermal printer head modulation plot, as in Figure 1.

The final technique modulates the heat pulse applied to the head of a commercially-available graphics thermal printer. A normal command sequence prints a single row of dots. For each print head position a reset signal is supplied to abbreviate each heat pulse in relation to the image intensity desired at that head position. The print head scans across the paper at only one rate, however, so storage of the input signal is required for plotting different full-scale heights. This has been accomplished using a 4-bit A/D converter and a simple microcomputer control circuit. The microcomputer also prints date, time and height scale information. A concern remains about the archival properties of thermal paper with regions of partially developed image, but no degradation has been noted over three months. Figure 4 shows an example of our thermal printer heat control method.

# SIMULATION OF TURBULENT AIRFLOW WITHIN AND ABOVE A TREE CANOPY

T. Yamada

---

Efforts have been made to produce a model that allows for the effects of complex topography on wind and turbulence fields. However, tall trees also affect the distribution of wind and turbulence in the lower atmosphere. It is well known that mean wind speed within a forest canopy is considerably smaller than above the trees owing to the surface drag induced by leaves, stems and branches. The kinetic energy lost by the mean flow is gained by turbulence. Tall trees also modify temperature profiles within and above a canopy. For example, during the day initial warming of the upper canopy results in an unstable layer above and a stable layer within the canopy. The stability structure is reversed during the night, because the rate of cooling due to longwave radiation is maximum in the upper canopy. The effects of a tall tree canopy (15-18 m) on wind, temperature and turbulence distribution are examined here with a one-dimensional version of the Level 2.5 turbulence-closure model (Mellor and Yamada, 1974).

Briefly, the net solar radiation $R_{Nh}$ at treetop is given by

$$R_{Nh} = (1 - \alpha_t)S + R_{L\downarrow} - R_{L\uparrow} \quad , \qquad (1)$$

where $\alpha_t$ is the tree albedo, S the solar radiation, $R_{L\downarrow}$ the incoming longwave radiation, and $R_{L\uparrow}$ the outgoing longwave radiation. The net radiation in a canopy is assumed to be given by (Uchijima, 1961; quoted in Ross, 1975, p. 52)

$$R_{Np} = R_{Nh} \exp(-kL(z)) \quad , \qquad (2)$$

where k denotes an extinction coefficient and L(z) the leaf area index. The heat energy balance equation within a canopy layer may be given approximately as

$$R_{Np} = H + LE + S_t = H(1 + \frac{1}{B}) + S_t \quad , \qquad (3)$$

where B = H/LE is the local Bowen ratio and $S_t$ the energy stored in the main stem and branches. All these terms are functions of height within the

canopy. According to Bradley et al. (1980), the heat storage $S_t$ in a plantation of 37-year old pine trees could be as large as 17% of the net radiation. The heat energy stored is expected to warm the air during nighttime in much the same way as heat energy stored in the soil. As a first approximation, the storage term is neglected by assuming that all the energy stored in the stems and branches becomes available immediately to heat the adjacent air. Under the conditions assumed, the internal heat energy equation is written as

$$\frac{D\Theta}{Dt} = \frac{\partial}{\partial z}(-\overline{w\theta}) + \frac{(1-\eta)}{\rho C_p}\frac{\partial R}{\partial z} + \frac{\eta}{\rho C_p}\left(1 + \frac{1}{B}\right)^{-1}\frac{\partial R_{Np}}{\partial z} \quad , \qquad (4)$$

where the Bowen ratio in a canopy is assumed to be constant with height, $\eta$ is the fraction of area covered by trees, and R is the longwave radiation flux without trees.

The effect of drag induced by trees is parameterized in a fashion similar to that used by Wilson and Shaw (1977); the equation of motion is modified as

$$\frac{DV_i}{Dt} = \ldots - C_d A U_i^2 \quad , \qquad (5)$$

and a turbulence energy equation is

$$\frac{D(q^2/2)}{Dt} = \ldots + C_d A\left[U^3 + V^3 + W^3\right] , \qquad (6)$$

where $C_d$ is a drag coefficient and A is a foliage area density function (the terms shown on the right-hand side constitute the modifications).

The vertical profiles of wind and temperature shortly after sunset with and without a tree canopy (Figure 1) illustrate the reduction in horizontal wind speeds within the canopy due to drag. The profiles of potential temperature over the canopy shows a minimum near treetop, while maximum cooling occurs at the ground for bare soil. Unstable stratification within the canopy and large wind shear near treetops result in relatively large turbulence as presented by the eddy viscosity coefficient profile in Figure 1. Turbulence for the bare soil case is negligible due to a surface inversion. Diurnal variations of wind speed (Figure 2) show wind maxima of 10

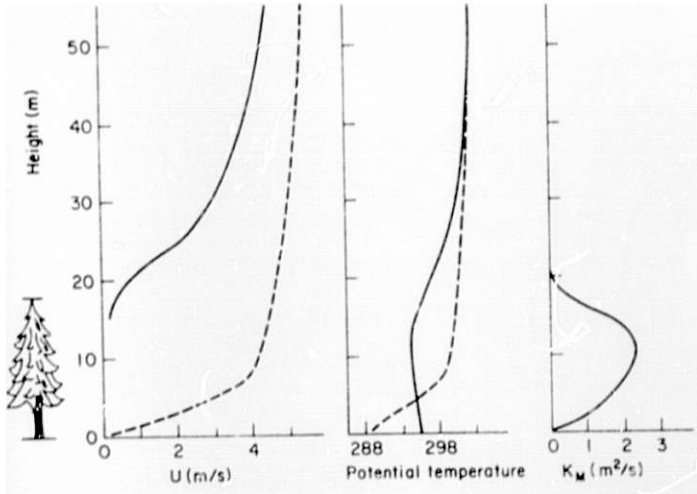


FIG. 1. Vertical profiles of simulated wind, potential temperature and eddy viscosity coefficient at sunset with (___) and without (---) trees in the model.

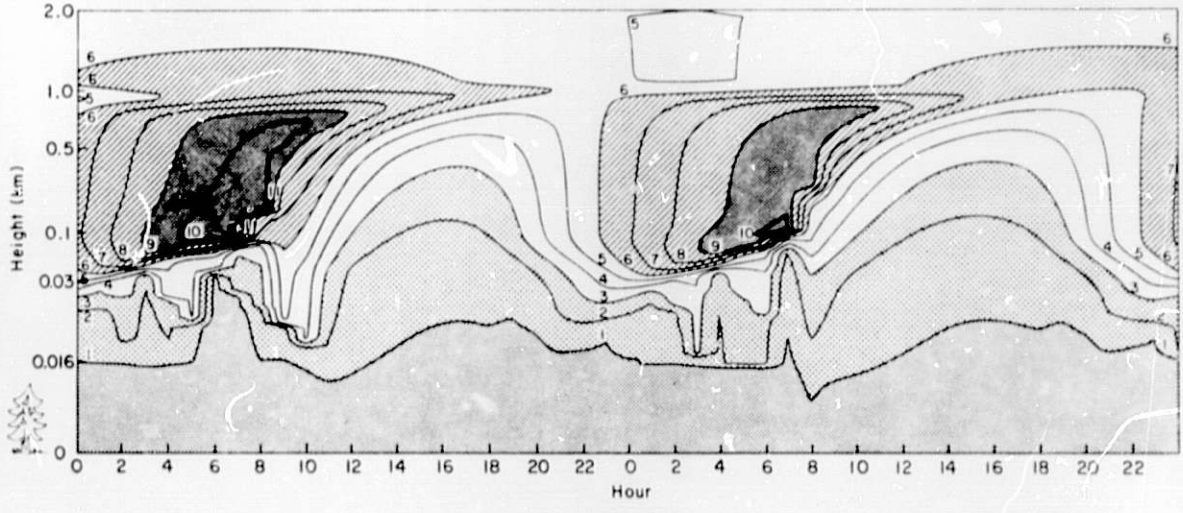


FIG. 2. Diurnal variations of simulated winds for the last 48 hr of a 4-day simulation.

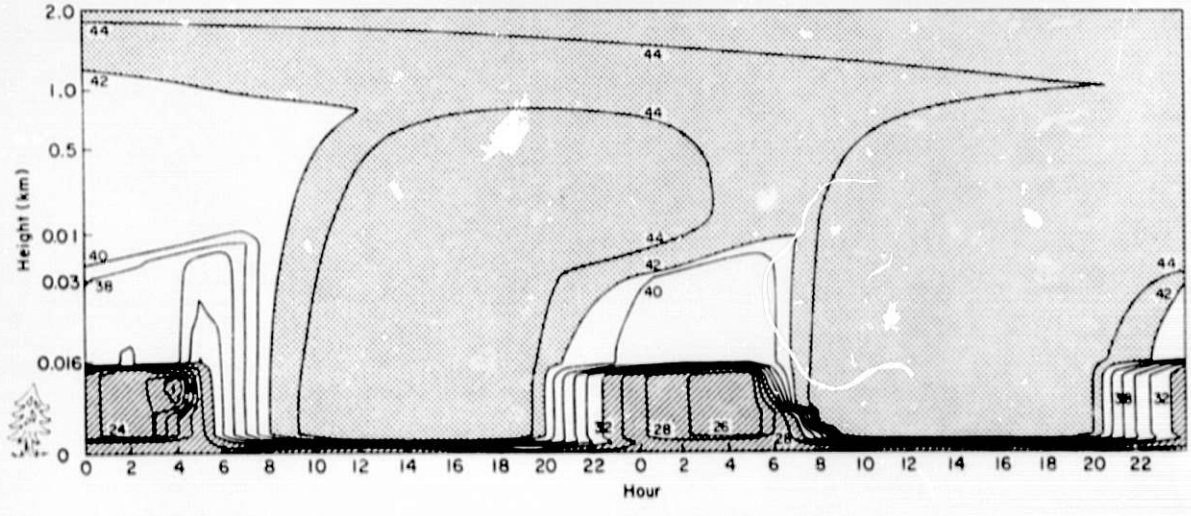


FIG. 3. Diurnal variations of simulated potential temperatures for the last 48 hr of a 4-day simulation.

to 11 m $s^{-1}$ at approximately 150 m near sunrise and light wind (< 5 m $s^{-1}$) during the day. Concurrent diurnal variations of potential temperature (Figure 3) display unstable layers within a canopy during the night and shallow stable layers near the ground during the day.

References


Bradley, E. F., O. T. Denmead, and G. W. Thurtell, 1980: Measurements of turbulence and heat and moisture transport in a forest canopy. Q. J. R. Meteorol. Soc., submitted for publication.

Mellor, G. L. and T. Yamada, 1974: A hierarchy of turbulence closure model for planetary boundary layer, J. Atmos. Sci. 31, 1791-1806.

Ross, J., 1975: Radiative transfer in plant communities. Vegetation and the Atmosphere, Vol. 1, J. L. Monteith, Ed., Academic Press, New York, pp. 13-55.

Wilson, N. R., and R. H. Shaw, 1977: A higher order closure model for canopy flow, J. Appl. Meteorol. 16, 1197--1205.

# A SIMULATION OF NOCTURNAL DRAINAGE FLOW IN SOUTHEAST AUSTRALIA

T. Yamada

---

A model based on simplified second-moment turbulence-closure equations has been used previously to simulate nocturnal drainage flow over the California Geysers area. The results agree generally with theoretical predictions for one-dimensional slope flow. However, wind speeds in the Geysers area observed with tethersondes are usually much smaller and more uniform with height than model simulations. It is possible that the measurement of wind profiles by tethersondes might have missed wind maxima confined to a thin layer (< 50m) near the surface because of a rather coarse vertical resolution. It is also speculated that the observed drainage flow might have been decreased considerably by drag induced by trees surrounding most observational sites. The effect of the drag associated with tree canopies is being included in the model as discussed elsewhere in this report (Yamada, 1980). This speculation is partially supported by recent measurements of drainage flow in southeast Australia over a slope with sparse tree coverage by Manins and Sawford (1979). Their wind profiles clearly show large maxima that are similar to the model simulations.

Here, the model simulations are compared with wind data collected over the Jeeralang Hills in Southeast Australia. As suggested by Manins and Sawford, nocturnal drainage flows developed along the sides of the valley might have converged into the main valley and affected significantly the wind profiles measured at a relatively flat site near the mouth of the valley (Figure 1). For simplicity, however, only the variations in a vertical cross section along the main slope are considered here. In other words, the terrain gradient is assumed to be zero perpendicular to the cross section, and thus, a two-dimensional version of the model (Yamada, 1981) can be used. Soil temperatures are determined by solving a heat conduction equation for soil layers and using as boundary conditions a heat energy balance equation at the ground and a specified constant temperature 50 cm below the surface (see Yamada, 1981 for details).

The initial wind profiles are assumed to be logarithmic with height at the inflow boundary and are adjusted elsewhere to satisfy mass continuity.

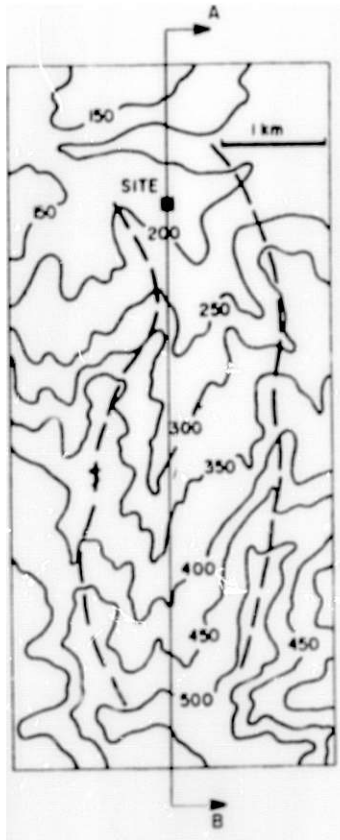


FIG. 1. Contours (meters) of the Jeeralang Hills in southeast Australia. Simulations are conducted over the slope indicated by the line A-B.

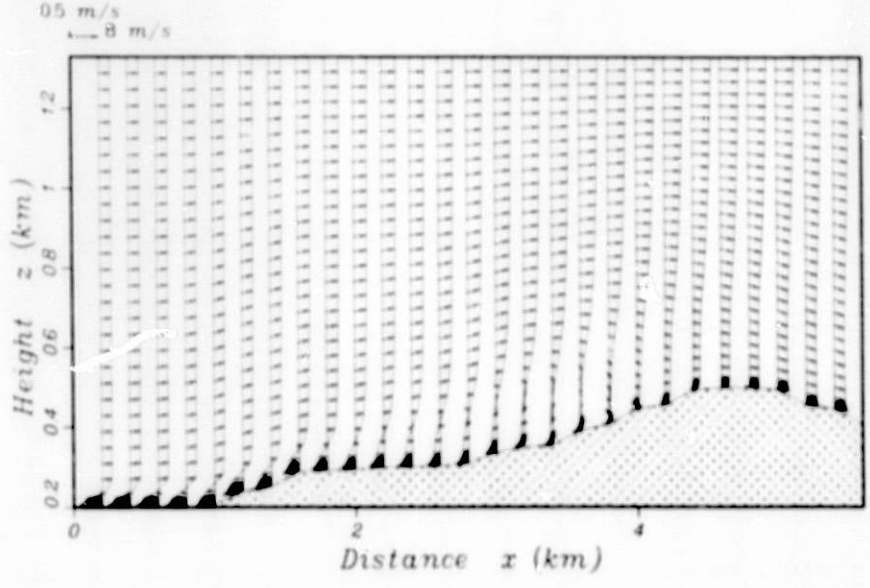


FIG. 2. Vertical profiles of simulated wind vectors.

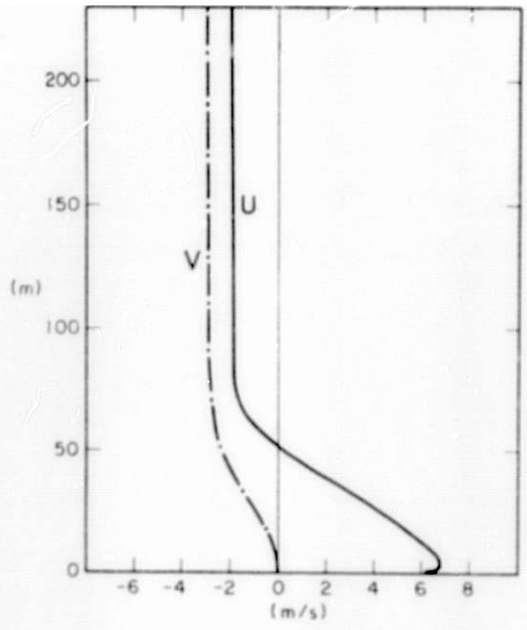


FIG. 3. Vertical profiles of simulated wind components parallel (U) and perpendicular (V) to the surface wind direction at an observational site.

The gradient of the initial potential temperature profile at the inflow boundary is assumed to be slightly stable. Simulation was initiated at midnight and continued for two and a half hours. Vertical profiles of horizontal wind component U are shown in Figure 2. Wind speeds in the upper layer decrease as the cross section slopes downward, satisfying mass continuity. It should be noted that the decrease is artificial and subject to the location of the upper computational boundary. On the other hand, wind profiles for the first two hundred meters above the ground show many complex features due to interaction between large-scale (imposed) and local-scale (computed) pressure gradients.

Major difficulties in obtaining analytical solutions of equations of motion for airflow over complex terrain arise from the invalidity of various assumptions used to simplify the governing equations for flat terrain. For example, the present simulation indicates that horizontal advection of momentum in the equation of motion, which vanishes over flat terrain, is the most important term, particularly when the ground slope changes. This fact alone makes it almost impossible to obtain analytical solutions for drainage flow because the advection term is nonlinear. The advection is found to be in close balance with the surface drag and the pressure gradient developed over a sloped surface. The remaining terms are found to be negligibly small as the flow reaches steady state.

Figure 3 shows vertical profiles of wind components parallel (U) and perpendicular (V) to the surface wind direction. The general features agree reasonably well with measured profiles (Figure 6 of Manins and Sawford, 1979), but details are different: for example, the observed crosswind component (V) was almost zero for the first 40 m above the ground and rapidly increased to 2 m $s^{-1}$ above that level. It is speculated that drainage flows developed over the side slopes (Figure 1) might have prevented the main drainage flow in the valley from veering with height. This hypothesis will be examined in the near future with a fine resolution, three-dimensional model.

## References


Manins, P. C., and B. L. Sawford, 1979: Katabatic winds: A field case. Q. J. R. Meteorol. Soc. 105, 1011-1025.

Yamada, T., 1980: Simulation of turbulent airflow within and above a tree canopy, this report.

Yamada, T., 1981: A numerical simulation of nocturnal drainage flow. J. Meteorol. Soc. Japan. 59, 108-122.

# DIURNAL VARIATION OF AIRFLOW OVER A TWO-DIMENSIONAL SYMMETRIC HILL

T. Yamada

---

In the following simulations, a two-dimensional version of a turbulence closure model (Yamada, 1981) reproduces qualitatively a diurnal variation of airflow over a sloped surface. The most important driving force of the model is the solar radiation, a major component of the surface energy budget. A nonvegetated soil surface is assumed. The resulting estimates of surface soil temperature provide a necessary atmospheric boundary condition for the equation of internal energy, which describes distribution of potential temperatures. If the rate of cooling or warming is assumed to be uniform along the surface boundary, then $\Delta\theta_v$, the deviation of potential temperature from the reference value, results in the horizontal pressure gradient in the equation of motion as

$$\frac{1}{\rho}\frac{\partial p}{\partial x} \approx \frac{-g}{\bar{H}\,\langle\theta_v\rangle}\frac{\partial z_g}{\partial x}\int_0^{\bar{H}}\left[\Delta\theta_v(0) - \Delta\theta_v(z')\right]dz' , \qquad (1)$$

where p is pressure, $\rho$ is air density, g is the acceleration of gravity, $z_g$ is the ground elevation, $\langle\theta_v\rangle$ is a reference virtual potential temperature that is a function solely of height, $\Delta\theta_v = \theta_v - \langle\theta_v\rangle$, x is the horizontal coordinate, and z' is a dummy variable representing a transformed height coordiate with a constant upper boundary $\bar{H}$.

Since the deviation of potential temperature from the reference value is maximum at the surface and decreases upward, the magnitude of the first term in the parenthesis is always greater than that of the second term. Consequently, the sign of the pressure gradient is opposite to the sign of $\Delta\theta_v$, assuming $\partial z_g/\partial x > 0$. For the nocturnal boundary layer developed over a sloped surface, $\Delta\theta_v$ is negative because of cooling from the ground. Therefore, a positive pressure gradient in the upslope direction develops and results in nocturnal drainage flow. The opposite case occurs during daytime where $\Delta\theta_v$ is positive because of warming from the ground, resulting in upslope flow.

Initially, extremely weak easterly flow and horizontally uniform potential temperature are assumed. Vertical profiles of simulated wind

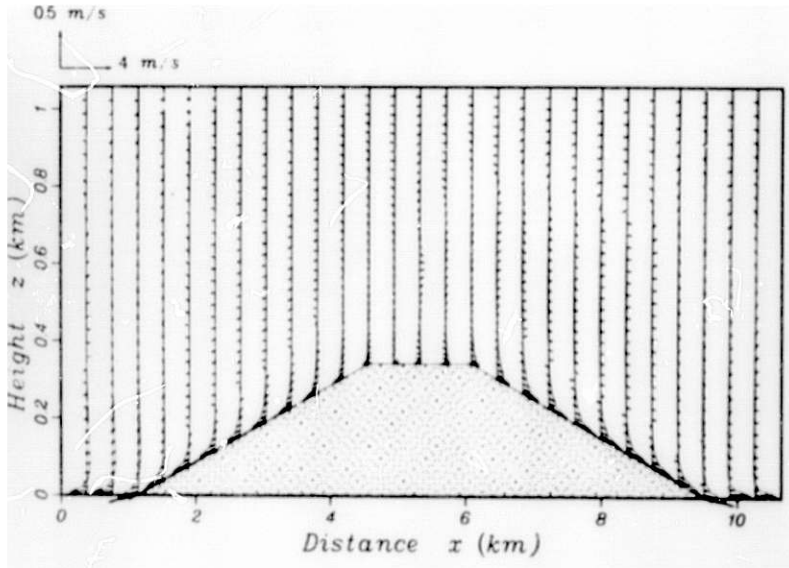


FIG. 1. Vertical profiles of simulated wind vectors at 0400 LST over a two-dimensional symmetric hill.

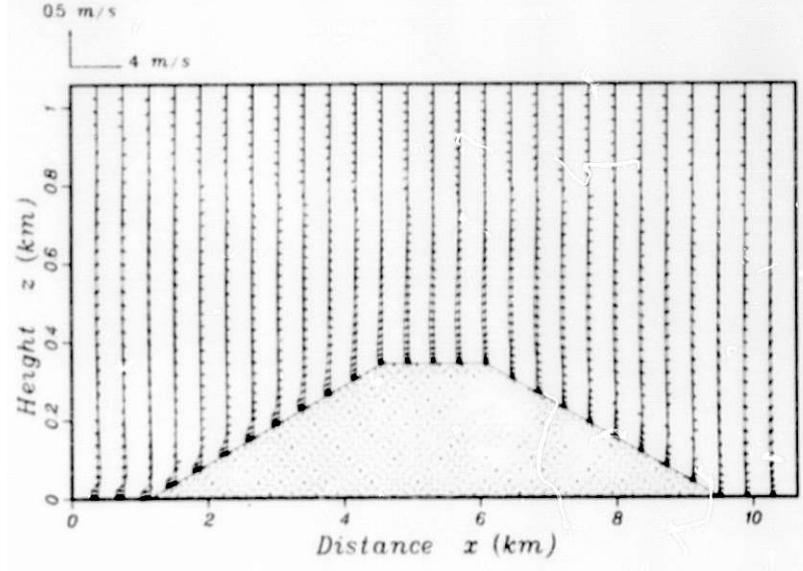


FIG. 2. Same as in Figure 1 except at 0700 LST.

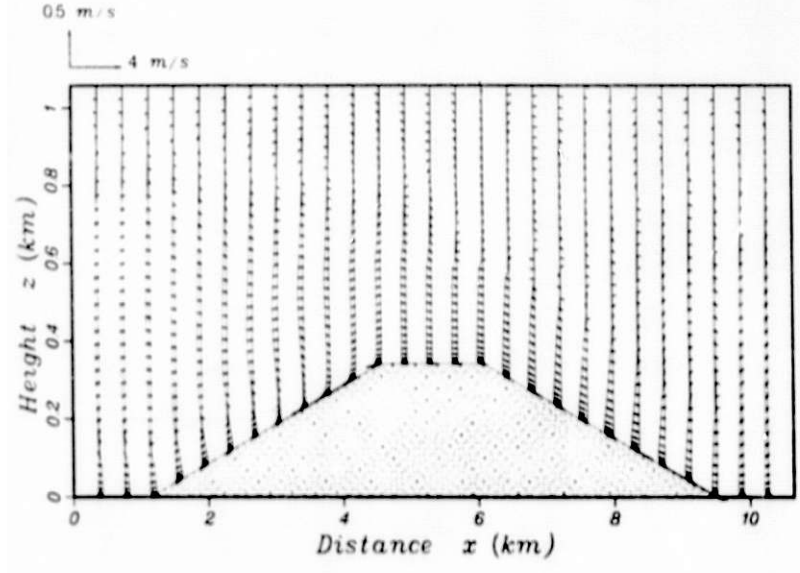


FIG. 3. Same as in Figure 1 except at 0800 LST.

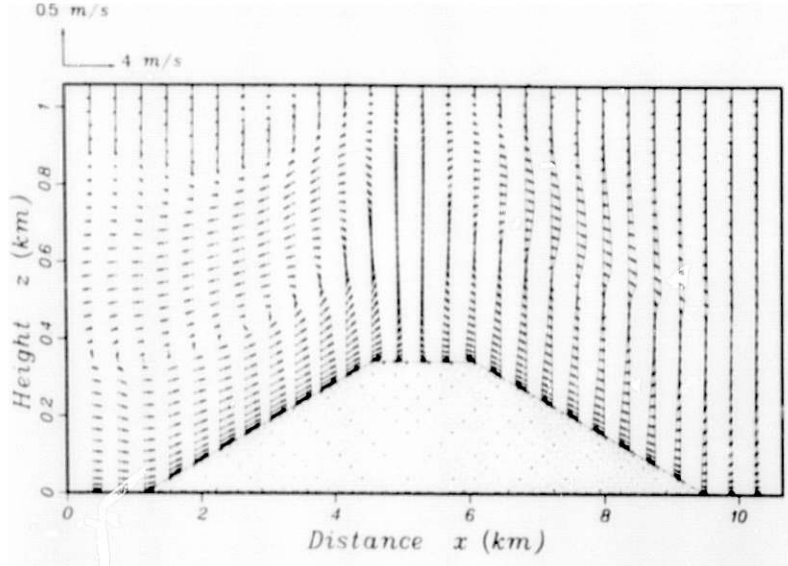


FIG. 4. Same as in Figure 1 except at 1000 LST.

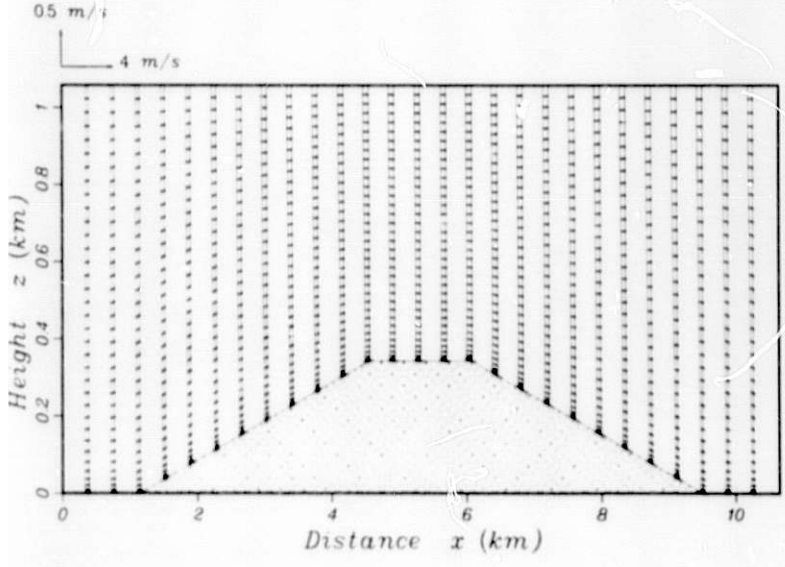


FIG. 5. Same as in Figure 1 except at 1900 LST.

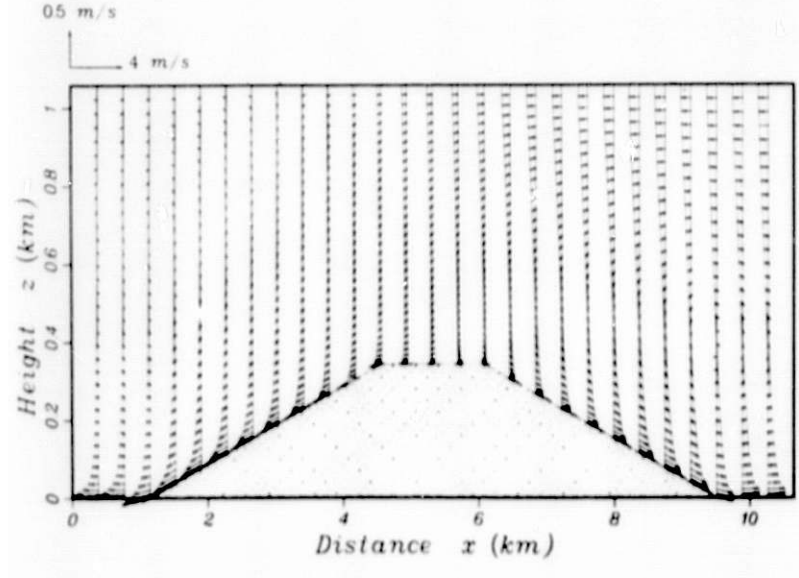


FIG. 6. Same as in Figure 1 except at 2400 LST.

vectors at 0400 LST (four hours after start of integration) exhibit nocturnal drainage flow developed over both slopes (Figure 1). A weak but deep return flow develops above the surface drainage flow in order to satisfy mass continuity. Shortly after sunrise, upslope flow develops over the eastern slope but drainage flow still continues over the western slope (Figure 2). Upslope flow develops over the western slope by 0800 LST (Figure 3), and reaches maximum intensity by 1000 LST (Figure 4). Note that the depth of the convective upslope flow is much deeper than that of the nocturnal drainage flow (as in Figure 1). Depth of the mixed layer increases with time, and wind profiles become uniform with height (Figure 5). After sunset (~ 1900 LST), longwave radiational cooling decreases surface temperatures and drainage flow develops (Figure 6).

Reference

Yamada, T., 1981: A numerical simulation of nocturnal drainage flow, J. Meteorol. Soc. Japan, 59, 108-122.

# NUMERICAL SIMULATION OF PARTICLE DISPERSION FROM EMISSIONS AT A HIGHWAY

C. M. Sheih

The anticipated increase in the number of diesel-powered automobiles would result in significantly increased emissions of respirable and potentially carcinogenic particulate matter. To study this problem, improved methods for predicting concentrations of particulate and gaseous pollutants over urban areas should be developed in parallel with research on the chemical characterization and the health effects of the emissions.

Conventional methods for modeling particle dispersion from highways make use of Gaussian models (e.g., Zimmerman and Thompson, 1975), but there are many problems associated with these models (see Egan and Mahoney, 1972, and Sheih, 1978). One of the most serious problems is in the treatment of particle coagulation, which consists of non-linear interactions that cannot be properly accounted for in a Gaussian model.

To overcome this and other problems, a finite-difference model has been developed; the model is used in the present study to evaluate the importance of particle coagulation during dispersion of emissions from a highway. Basically, the model solves a system of finite difference equations of diffusion. Each equation accounts for the budget of a certain size range of particles and contains the effects of mean wind advection, turbulent diffusion, and gravitational settlement, as well as coagulation. The model simulates particle dispersion for an experiment reported by Whitby et al. (1976).

Figure 1 shows the distribution of particle concentration (volume per volume) as a function of particle diameter. The curve for x = 0 m is derived from the roadside observation of Whitby et al. (1976) , while particle distributions at 100 and 400 m downstream are produced by numerical simulation. The trimodal distribution appears to be due to the existence of three distinctive mechanisms, i.e., combustion, aging, and mechanical production. The dashed lines result from the assumption that no particles with diameters larger than 1 μm (supermicron particles) exist at x = 0 m, whereas the solid lines portray a complete trimodal distribution in the corresponding initial condition. Elimination of the supermicron particles from the initial atmosphere reduces the number of agents that collect

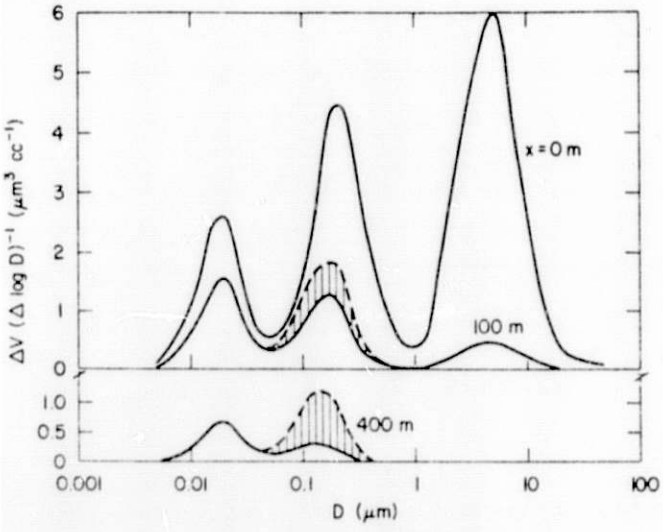


FIG. 1. Distributions of particle concentrations as functions of particle diameter for an observation at roadside (x = 0 m) and for numerical predictions at downstream distances x = 100 and 400 m. Dashed lines are predictions assuming no particles larger than 1μm.

submicron particles and apparently results in an increase in submicron particles downstream. The effect is pronounced on the aging mode (0.05 to 1 μm diameter) but almost negligible on the combustion mode (smaller than 0.05 μm diameter). The latter is not surprising because the aging mode, which has many more particles than the supermicron mode, dominates coagulation and disappearance of the combustion mode particles, since the rate of coagulation is more dependent upon the number of particles than upon the volume occupied. The shaded areas, representing the difference between the cases with and without supermicron particles, show that the increases in the volume of submicron particles due to absence of coagulation to supermicron particles are about 20 and 50% at 100 and 400 m downstream from the roadside, respectively. Hence, when coagulation has such a significant effect on particle concentration, extreme caution should be made in using a Gaussian model for predicting particle dispersion.

References

Egan, B.A., and J. R. Mahoney, 1972: Numerical modeling of advection and diffusion of urban area source pollutants, J. Appl. Meteorol. 11, 312-322.

Sheih, C. M., 1978: A puff-on-cell model for computing pollutant transport and diffusion, J. Appl. Meteorol. 17, 140-147.

Whitby, K. T., D. B. Kittleson, B. K. Cantrell, N. J. Barsic, D. F. Dolan, L. D. Travestad, D. J. Nieken, J. L. Wolf, and J. R. Wood, 1976: Aerosol size distributions and concentrations measured during the General Motors/Environmental Protection Agency Sulfate Experiment, Selected EPA Research Papers, EPA-600/3-76-035, 29-80.

Zimmerman, J. R. and R. S. Thompson, 1975: User's guide for HIWAY: A highway air pollution model, Environmental Protection Agency, Research Triangle Park, North Carolina 27711, publication EPA-650/4-74-008 (NTIS PB-23994/AS).

# PRELIMINARY MEASUREMENTS OF AEROSOL, TURBULENCE, AND MEAN WIND VELOCITY IN A STREET CANYON

C. M. Sheih and F. T. DePaul

---

Street canyons in urban areas are known to be isolated from upper air flow and to trap pollutant emissions for extended periods. Because of a lack of simple methods to estimate pollutant concentrations in the street, most numerical models treat the city as a flat surface in calculation of concentrations at street level. A simple parameterization to relate pollutant concentration at street level to its ambient or roof-level value was attempted in an earlier study by Sheih (1979). The present report presents some preliminary results of field experiments designed to calibrate the constants involved in the parameterization.

The experiments were conducted on a section of Clark Street (oriented north-south) between Congress and Harrison Street (both east-west) in downtown Chicago. For measurements of vertical profiles, a hot-wire probe and tubing for intake of air were moved up and down by a pulley attached to the end of a boom, anchored to the roof about 2 m from the building wall. The polyester tubing was about 70 m long, with one end for air intake placed about 20 cm from the hot-wire probe and the other end attached to air quality analyzers housed in a motor home parked on the side of the street. Concentrations of particles were measured with an electrical aerosol analyzer for submicron particles and a Climet optical particle counter for supermicron particles. Since the tubing was found to be too long for passage of supermicron particles without serious deposition loss, only measurements of submicron particles are presented.

Figure 1 shows sample measurements of thirty-minute average profiles of mean wind velocity, standard deviation of turbulent wind components and total submicron particle volume concentration taken on a cloudy, windy afternoon in November, 1980. The mean wind inside the street canyon is northerly (along the street) and fairly constant at 4 m $s^{-1}$ from 8 m height to roof level. Below 8 m, the mean wind decreases to 3 m $s^{-1}$ at pedestrian level. This reduction is attributed to traffic movement, which is against the wind on the one-way street, as well as to surface drag. The wind velocity at

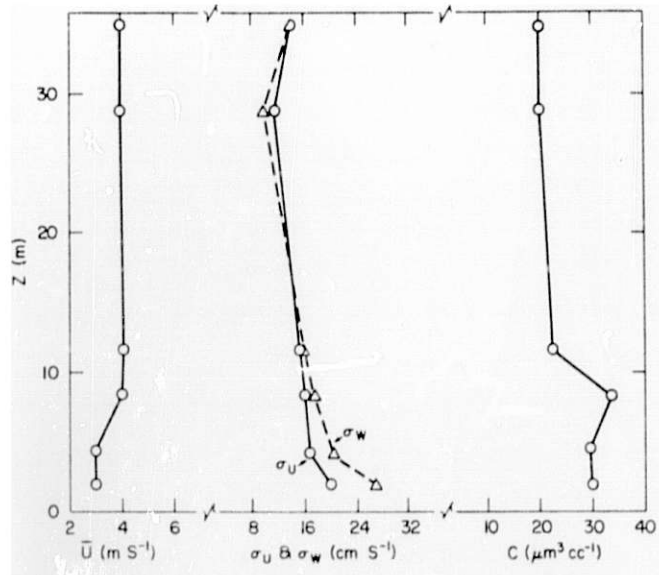


FIG. 1. Mean wind velocity u, turbulence intensities $\sigma_u$ (mean wind component) and $\sigma_w$ (vertical component), and particle volume concentration c, all as functions of height.

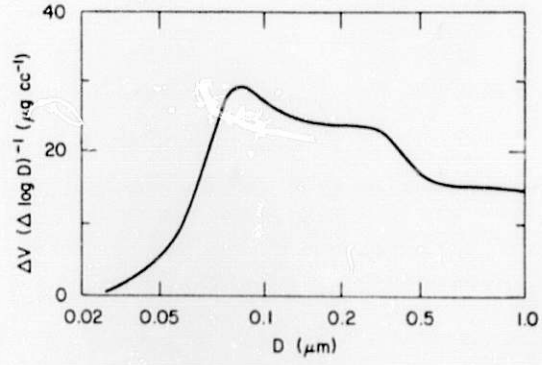


FIG. 2. Particle volume distribution at pedestrian height in a street canyon.

2 m above the roof (not shown here) is northeasterly at 6 m s$^{-1}$. Turbulence intensities are largest near pedestrian level, most likely owing to mechanical production in automotive wakes, which generate velocity fluctuations more vertically than horizontally oriented, as evidenced in the figure. Turbulence intensities decrease as height increases, except for a slight increase at roof level, possibly because of larger shear production there. The particle concentration is 50 % greater at pedestrian level than roof level. However, maximum value occurs at about 8 m, which may be due to buoyant plume rise of automotive exhaust.

A plot of the sample volume concentration of submicron particles as a function of particle diameter at street level (Figure 2) shows that the major contributions are from a particle size range of 0.06 to 0.5 μm; the peak value is at about 0.08 μm. Our results could be due to resuspension of particles caused by automotive movements in a relatively confined street canyon, thus making more supermicron particles available for coagulation with submicron particles.

Reference

Sheih, C. M., 1979: Preliminary theoretical analysis of pollutant dispersion in a two-dimensional street canyon, Argonne National Laboratory Radiological and Environmental Research Division Annual Report ANL-79-65 Part IV, pp. 10-11.

# EDDY-CORRELATION MEASUREMENTS OF PARTICLE FLUXES OVER LAKE MICHIGAN

M. L. Wesely and R. M. Williams

Several experiments over Lake Michigan have been conducted since autumn of 1978 in order to determine the eddy-correlation flux of submicron particles to large water bodies. The first of these has been described by Williams et al. (1979) but, as reported, the speeds during the measurements were too low to expect the accuracy of the techniques employed to be adequate. Here, results are given from four more-successful measurement periods, when similar techniques were applied in higher wind speeds.

As explained by Williams et al., a parameterization of the deposition velocity $v_d$ for submicron particles is sought, so that the total amount of potentially harmful substances entering the Great Lakes by dry deposition might be more easily estimated. The research actually focuses on a parameterization of the resistance $r_{sp}$ to the transfer of particles through the gaseous interfacial sublayer in immediate contact with the water surface. Then the flux (positive when directed upward and opposite to $v_d$ in polarity) can be calculated as

$$F = -v_d\chi = (r_{sp} + r_a)^{-1} \chi\zeta \ , \qquad (1)$$

where $\chi$ is the concentration, $r_a$ is the aerodynamic resistance above the sublayer to vertical flux, and $\zeta = F/|F|$ is applied to ensure that the resistance remains positive. During application of parameterizations, $r_a$ is estimated from meteorological information, and is readily calculated by use of atmospheric variables directly measured during field experiments.

Two sensors were used to measure the fluctuations of particle concentration for eddy correlation. The charger, a device on loan from Washington University in St. Louis, measured particles primarily of diameter 0.03 to 0.1 μm, and a commercially-available nephelometer detected particles primarily 0.3 to 1.0 μm in diameter. Figure 1 shows the results; all values of $F/\chi$ have been adjusted to represent those that would have been found in atmospherically-neutral conditions (see Wesely et al., 1981, for some of the appropriate formulations).

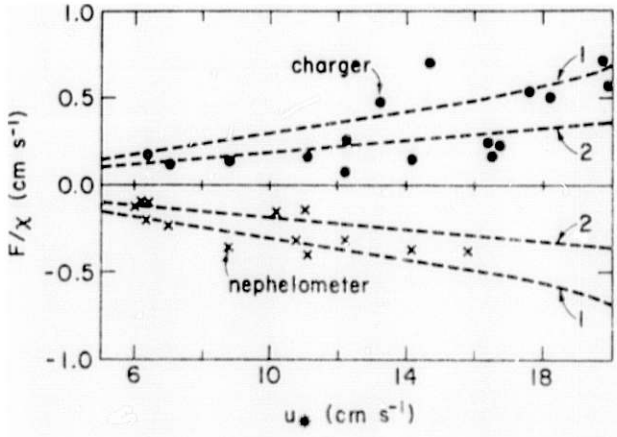


FIG. 1. Values of $F/\chi = -v_d$ versus the friction velocity $u_*$ computed from hourly averages of measurements above Lake Michigan. The curves are (1) computed for $r_{sp}$ equal to zero and (2) $r_{sp}$ given by Eq. 2.

The most evident feature of the data is that the charger particle fluxes are directed upward, away from the surface, and the nephelometer particle fluxes are directed toward the surface. That is, it appears that the surface is a source of the smaller particles but that the largest submicron particles are being removed from the atmosphere. The next most evident feature is that the data lie not great distances from the curves drawn for $r_{sp}$ equal to zero. Hence, in these light to moderate winds, $r_{sp}$ seems quite small, smaller than estimates traditionally assumed.

The curves marked 2 in Figure 1 show the values of $F/\chi$ if the estimates of $r_{sp}$ resulting from suggestions by Wesely (1980) are used. That is, $r_{sp}$ is given as

$$r_{sp} = (ku_*)^{-1} \{1 + \ln(z_o\ k\ u_*/D_p)\} , \qquad (2)$$

where k is the von Karman constant, $z_o$ is the surface roughness length scale, $u_*$ is the friction velocity, and $D_p$ is the particle diffusivity in stagnant air. Clearly, the scatter in the data do not allow for a definite test of Eq. 2, or even of the assumption made by Sheih et al. (1979) that $r_{sp}$ is equal to 1.0 s $cm^{-1}$ for all wind speeds.

A perplexing question posed by the data in Figure 1 concerns the mechanism(s) causing the charger particle fluxes to appear to be directed upward. This behavior has been observed over land as well, over smooth wet surfaces or during atmospherically stable conditions (Wesely and Hicks, 1979). It seems unlikely that the emission of very small particles is such a common feature; perhaps at the heights of measurement, typically 5 to 10 m,

the upward flux of particles is not representative of the fluxes much closer to the surface. For example, gases released from the surface might be rapidly converted to very small particles. The nephelometer data on the other hand, might be explained simply by the remark that the value of $r_{sp}$ is small. Perhaps it is sufficient to assume that $r_{sp}$ is 1.0 s cm-1, as has been done by Sheih et. al. (1979), for the bulk of submicron particulate material over water. Equation 2 or any other formulation that finds that $r_{sp}$ is small provides reasonable explanation also, as far as can be discerned from the data shown in Figure 1.

References


Sheih, C. M., M. L. Wesely and B. B. Hicks, 1979: Estimated dry deposition velocities of sulfur over the eastern United States and surrounding regions, Atmos. Environ. 13, 1361-1368.

Wesely, M. L. and B. B. Hicks, 1979: Dry deposition and emission of small particles at the surface of the earth, Fourth Symposium on Turbulence, Diffusion and Air Pollution, Reno, NV, American Meteorological Soc., pp. 510-513.

Wesely, M. L., 1980: Comments on "Bulk parameterization of air-sea exchanges of heat and water vapor including the molecular constraints at the interface," J. Atmos. Sci. 37, 2798-2800.

Wesely, M. L., D. R. Cook and R. M. Williams, 1981: Field measurements of small ozone fluxes to snow, wet bare soil, and lake water, Boundary-Layer Meteorol., in press.

Williams, R. M., M. L. Wesely and B. B. Hicks, 1979: Preliminary eddy-correlation measurements of momentum, heat and particle fluxes to Lake Michigan, Argonne National Laboratory, Radiological and Environmental Research Division Annual Report ANL-78-65 Part III, pp. 82-87.

# PRELIMINARY MEASUREMENT OF $CO_2$ FLUX

M. L. Wesely, D. R. Cook, and R. M. Williams

A reliable determination of possible climate changes associated with increased atmospheric $CO_2$ requires evaluation of the atmospheric $CO_2$ budget, which includes global surface $CO_2$ fluxes as well as emissions from fuel combustion and other activities of man. While the air-surface exchange rates of $CO_2$ are quite complex spatially and temporally, better knowledge of one physical process, the transfer of $CO_2$ through the aqueous sublayer at the air-sea interface, would significantly aid predictions of $CO_2$ concentrations. Transfer through this sublayer results in vast exchanges of $CO_2$ globally, but transfer can be strongly limited locally by the poor mixing in the sublayer and the small molecular diffusivity of $CO_2$ in water. A promising method of measuring $CO_2$ flux is being tested in order to derive better parameterizations of transfer across the air-sea interface.

Eddy-correlation techniques are used to measure $CO_2$ flux in the atmospheric surface layer, in much the same manner as has been used to study ozone flux over water (Wesely et al., 1981). A fast-response $CO_2$ sensor assembled at Argonne from commercially-available components provides values of concentration $\chi$, so that the vertical flux $F_c$ can be computed as

$$F_c = \overline{w' \chi'} + \overline{w}\,\overline{\chi} \quad , \qquad (1)$$

where w is the vertical wind speed, the overbars represent time averages, and the primes indicate deviations from the means. In the proper experimental conditions, $F_c$ is the vertical flux density of $CO_2$ that occurs at the surface, even though the actual measurement is made several meters above the surface.

The flux of $CO_2$ over fresh water measured on two expeditions on Lake Michigan in 1980 is shown in Table 1. In an arrangement similar to that described in a previous annual report (Williams et al., 1979), the eddy-correlation measurements were taken from a fixed tower while the R/V Ekos was anchored nearby to supply electrical power and a platform for some of the signal-processing electronics. During these measurements, winds were light to moderate, and capillary waves were present but not breaking waves. As seen in Table 1, the $CO_2$ fluxes are directed upward, away from the surface, for most of the evening and nighttime hours. After omission of the last three values,

Table 1. Hourly averages of $CO_2$ fluxes measured at Lake Michigan

| Time CST (center) | $CO_2$ concentration ppm | $CO_2$ flux, $\mu g\ m^{-2}\ s^{-1}$ |
|---|---|---|
| 18 June 1980 | | |
| 0430 | 360 | -3.2 |
| 0530 | 360 | 8.3 |
| 0630 | 360 | 3.2 |
| 27-28 August 1980 | | |
| 1630 | 336 | 8.3 |
| 1730 | 330 | -3.3 |
| 1830 | 325 | 2.8 |
| 1930 | 316 | 6.2 |
| 2030 | 315 | 0.0 |
| 2130 | 313 | 3.8 |
| 2230 | 310 | -1.2 |
| 2330 | 310 | 9.3 |
| 0030 | 3-9 | 8.8 |
| 0130 | 310 | 2.2 |
| 0530 | 319 | 0.5 |
| 0630 | 322 | 3.3 |
| 0730 | 330 | -7.5 |
| 0830 | 344 | -17.7 |
| 0930 | 341 | -9.8 |

obtained during 0700 to 1000 hr, the average $CO_2$ flux is 3.3 ± 1.1 $\mu g\ m^{-2}\ s^{-1}$. The change in flux direction at about 0700 might be (1) an artifact due to the effects of advection or (2) a reality associated with a changing concentration gradient in the aqueous sublayer. Future experiments will be necessary to isolate the important factors.

An important question is whether the accuracy of $CO_2$ flux measurements will be adequate to measure the very small $CO_2$ fluxes expected in future experiments over open water. An estimate of the accuracy obtained can be found by examination of the $CO_2$ fluxes already measured over Lake Michigan. From Table 1, fifteen hour-long samples of $CO_2$ flux produce a standard error of 33% of the mean "emission" velocity (flux divided by concentration) of 0.0006 cm $s^{-1}$. With a little manipulation, it can be shown that for the $CO_2$ measurements the standard error on emission velocity is about $0.0008/n^{1/2}$, where n is the number of one-hour data-collection periods.

Calculations based on the parameterizations reviewed by Wesely (1980) indicate that a gas-phase emission or deposition velocity of 0.0005 cm $s^{-1}$ might be near the maximum found above a nonreactive water surface when wind speeds are 2 m $s^{-1}$ at a height of 10 m. In this case, nearly 260 one-hour samples are needed to reduce the standard error to 10% of the mean. In future experiments, perhaps 5 to 10 one-hour data-collection periods at fairly narrow ranges of wind speeds can be obtained during a typical expedition employing one $CO_2$ sensor. Therefore, the standard errors will be about 0.0004 cm $s^{-1}$ or 2.4 μg $m^{-2}$ $s^{-1}$. This implies that the relative accuracy might be no better than ± 80% of the fluxes at the lowest wind speeds (2 m $s^{-1}$ at a 10 m height) that can be successfully utilized with the present eddy-correlation apparatus. As the wind speed increases, the relative standard error is reduced considerably. At 8 m $s^{-1}$, when breaking waves start to appear, the standard errors should be less than 20% of the mean. These estimates, however, are conservative because the entire data set of emission or deposition velocity versus wind speed should increase the statistical significance of the results notably. Also, this is all postulated on the use of only a single $CO_2$ sensor and on the assumption that the aqueous resistance to transfer is controlled entirely by physical mechanisms, none chemical or biological. Enhanced transfer would result in smaller relative standard errors.

The preliminary results presented here have encouraged more extensive experiments over large bodies of water. Because of the frequent occurrence of breaking waves in ocean waters, transfer during high wind speeds cannot be ignored. A new theoretical approach may have to be developed in order to parameterize the effects of breaking waves on transfer.

## References

Wesely, M. L., 1980: Comparisons of surface-renewal predictions with data, Winter Annual Meeting of the American Society of Mechanical Engineers, November 21, 1980, Chicago, Illinois.

Wesely, M. L., D. R. Cook, and R. M. Williams, 1981: Field measurements of small ozone fluxes to snow, wet bare soil, and lake water, Boundary Layer Meteorol., in press.

Williams, R. M., M. L. Wesely, and B. B. Hicks, 1979: Preliminary eddy-correlation measurements of momentum, heat and particle fluxes to Lake Michigan, Argonne National Laboratory Radiological and Environmental Research Division Annual Report ANL-78-65 Part III, pp. 82-87.

# TEMPERATURE TRENDS IN NORTHERN ILLINOIS

D. R. Cook

A strong cooling trend has been observed since 1930 at Purdue University in West Lafayette, Indiana (Agee, 1980). Temperature data from the 11 stations in Northern Illinois (N.I.), shown in Figure 1, including the thirty-year record at Argonne National Laboratory, are analyzed here to investigate the trend of temperature over the same period. Eleven-year averages of temperature, plotted for each decade midyear, are shown in Figure 2, in addition to a N.I. average for eight stations outside metropolitan Chicago, the Purdue measurements and the North American (N.A.) average (Agee, 1980). The N. A. temperature decrease of 0.4° C over the fifty-year study period is less than that of N. I. (1.1° C), indicating that N. I. has undergone greater cooling than have other areas of the continent.

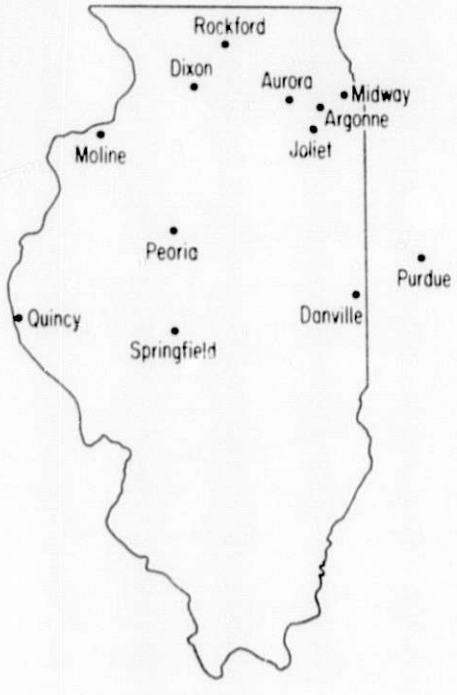


FIG. 1. Stations from which temperature were obtained.

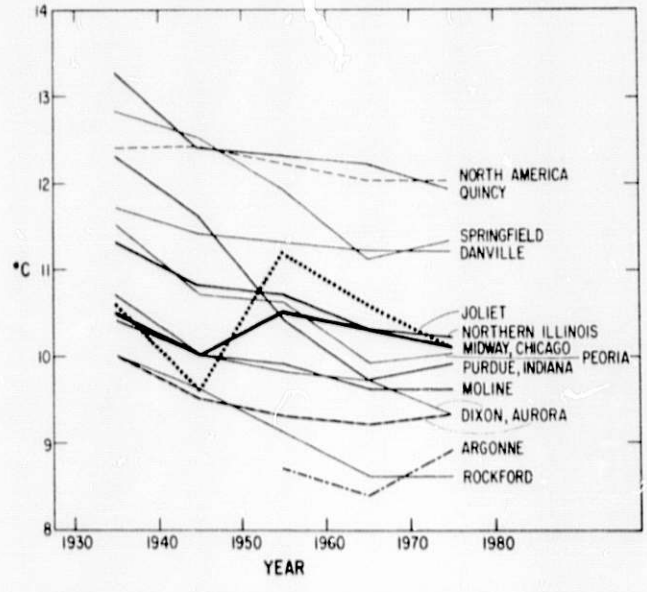


FIG. 2. Temperature trend by decades, 1930 through 1979. Curve labelled Northern Illinois is an average of eight stations outside metropolitian Chicago. The North American average is from Agee (1980).

Inspection of the data reveals that the fifty-year trends are similar for 9 of the 11 stations in N. I. Between the 1930's and 1940's, the temperature dropped sharply at each station, a regional feature contrasting

with the lack of change over N. A. as a whole. The temperature decrease in N. I. between the 1940's and 1950's was generally smaller than during the previous decade and consistent with the N. A. trend. A more pronounced drop occurred between the 1950's and 1960's in N. I., similar to the drop of two decades before. Between the 1960's and 1970's, the temperature drop resembled the drop of twenty years before. During the 1970's the temperature increased slighly between 1970 and 1975, but decreased slightly thereafter (detail not plotted). For this reason, apparently, some stations show a decrease in temperature from the 1960's to the 1970's, while other show an increase or no change, the latter situation being consistent with the N. A. trend.

Joliet Municipal Airport and Midway Airport in Chicago were the only two stations studied that recorded temperature trends radically different from the N. I. trend. Anomalies occurred at both stations between the 1940's and 1960's. Unfortunately, no information is available about sensor placement at Joliet Municipal Airport. Urbanization is not responsible for the trend anomaly since the airport remained well southwest of the urban area during the period in question. The anomalies at Midway are most likely a result of movement of the sensor site; in early 1941 the sensor was moved from the roof of a hangar office to a plot of grass fifteen meters north, in order to reduce data bias. Increased aircraft traffic resulted in the sensor again being moved, in the early 1960's, to a more remote location at the airport.

The thirty-year record at Argonne is consistent with the N. I. trend. Although slightly south of Dixon and Aurora, Argonne recorded significantly lower temperatures. This is probably explained by the fact that the temperature at Argonne was measured over a rural area, whereas at Dixon and Aurora measurements were made in downtown areas.

Three of the four stations located midstate, longitudinally, in N. I. experienced the greatest temperature decreases during the fifty-year study period: Springfield, 1.5° C; Peoria, 1.5° C; and Rockford, 1.4° C. Quincy, in the west-central part of the state, experienced a 1.4° C decrease. Danville (0.5° C) and Aurora (0.7° C) had the smallest decreases. The small Danville decrease is in sharp contrast to the 2.4° C decrease at Purdue, fifty miles to the east. Since the Purdue record closely resembles that at Springfield (to the west of Danville), the Danville record may be of questionable accuracy, even though it is consistent with the N. I. trend. The

variations of temperature trend between stations reflect differences in the effects of geography, instrument site location and measurement techniques. The N. I. average should be a better indication of the regional temperature trend than any single station.

## References


Agee, E. A., 1980: Present climatic cooling and a proposed causative mechanism, Bull. Am. Meteorol. Soc., 61, 1356-1367.

Climatological Data: Illinois Section and Local Climatological Data: Annual Summary with Comparative Data, 1930 through 1979. (available from the Nationl Climatic Center, Ashville, N.C.).

# SOURCE/RECEPTOR TRANSFER MATRICES

J. D. Shannon

Source/receptor transfer matrices represent results from simulations of Long-Range Transport (and deposition) of Air Pollutants (LRTAP) in a form convenient for investigation of emission scenarios. The (n × m) transfer matrix expresses the effect of a normalized emission from each of n sources upon each of m receptor areas where, for example, the effect can be average $SO_2$ or $SO_4^=$ concentration or cumulative wet or dry deposition of total sulfur. If an emission scenario can be described in a (1 × n) emission vector, then multiplication of the vector times the matrix produces a (1 × m) effects vector. On a digital computer the scenario examination requires less than one second for computation.

There are two major difficulties in interpretation of transfer matrix results. The first is that the matrix merges the effects of a particular meteorological data set with a specific combination of model assumptions; sensitivity testing requires recalculation of the matrix. The second is inadequate resolution when source and receptor areas coincide. This can be overcome by increasing the dimensions of the matrix and then combining results, but that is cumbersome if the matrix is large initially. Since the normalized effects of source areas on collocated receptor areas (the diagonal elements of the matrix) are the largest elements of the matrix, special care must be taken in their interpretation.

If one wishes to examine the combined effect of many sources upon a large area, contoured plots derived from values computed for regularly spaced grid points are most useful. However, if one wishes to examine the effect of a single source region upon a single receptor region, results can be read from an element of the transfer matrix and scaled by the actual emission rate. An example of a transfer matrix is shown in non-normalized form in Table 1.

A feature of transfer matrices is that they can be (and are) used by persons untutored in LRTAP modeling. Whether that is an advantage or a disadvantage remains to be seen. While the simple mathematical form of a transfer matrix allows the method to be used in objective optimization of emission strategies, it is a case of "building one's house upon the sand" unless the LRTAP model is scientifically sound.

Table 1. Example of source-receptor transfer matrix for reduction in cumulative dry deposition of total sulfur (g $m^{-2}$) for July-August

Reduction in $SO_2$ emission in tons/day by source region

| Receptor | SE PA 7. | C PA 6. | W PA 14. | NE WV 176. | SW WV 42. | E KY 225. | W KY 316. | S IL 230. | N IL 206. | N IN 83. | S IN 199. | S OH 272. | NE OH 100. | NE OH 58. | Total 1934. |
|---|---|---|---|---|---|---|---|---|---|---|---|---|---|---|---|
| ME | 0.0001 | 0.0000 | 0.0001 | 0.0004 | 0.0001 | 0.0003 | 0.0004 | 0.0002 | 0.0004 | 0.0002 | 0.0003 | 0.0006 | 0.0004 | 0.0002 | 0.0036 |
| White MT | 0.0001 | 0.0001 | 0.0001 | 0.0007 | 0.0001 | 0.0004 | 0.0005 | 0.0003 | 0.0005 | 0.0003 | 0.0004 | 0.0008 | 0.0006 | 0.0003 | 0.0052 |
| VT | 0.0002 | 0.0001 | 0.0001 | 0.0009 | 0.0001 | 0.0006 | 0.0007 | 0.0004 | 0.0006 | 0.0004 | 0.0005 | 0.0011 | 0.0009 | 0.0004 | 0.0071 |
| NH | 0.0002 | 0.0001 | 0.0001 | 0.0011 | 0.0002 | 0.0007 | 0.0006 | 0.0003 | 0.0005 | 0.0003 | 0.0005 | 0.0012 | 0.0008 | 0.0003 | 0.0070 |
| MA | 0.0003 | 0.0001 | 0.0002 | 0.0015 | 0.0002 | 0.0008 | 0.0007 | 0.0004 | 0.0005 | 0.0003 | 0.0005 | 0.0015 | 0.0010 | 0.0004 | 0.0085 |
| RI | 0.0005 | 0.0002 | 0.0002 | 0.0020 | 0.0003 | 0.0011 | 0.0008 | 0.0004 | 0.0006 | 0.0004 | 0.0006 | 0.0019 | 0.0012 | 0.0004 | 0.0105 |
| CT | 0.0006 | 0.0002 | 0.0002 | 0.0022 | 0.0003 | 0.0011 | 0.0009 | 0.0004 | 0.0006 | 0.0004 | 0.0007 | 0.0020 | 0.0013 | 0.0005 | 0.0116 |
| Adirond | 0.0002 | 0.0001 | 0.0002 | 0.0009 | 0.0001 | 0.0006 | 0.0007 | 0.0005 | 0.0008 | 0.0005 | 0.0006 | 0.0011 | 0.0010 | 0.0004 | 0.0077 |
| W NY | 0.0004 | 0.0004 | 0.0004 | 0.0018 | 0.0003 | 0.0011 | 0.0012 | 0.0007 | 0.0011 | 0.0007 | 0.0009 | 0.0021 | 0.0022 | 0.0008 | 0.0140 |
| SE NY | 0.0011 | 0.0003 | 0.0003 | 0.0031 | 0.0005 | 0.0015 | 0.0011 | 0.0005 | 0.0007 | 0.0005 | 0.0009 | 0.0027 | 0.0017 | 0.0006 | 0.0155 |
| NJ | 0.0012 | 0.0004 | 0.0004 | 0.0043 | 0.0006 | 0.0019 | 0.0013 | 0.0005 | 0.0007 | 0.0005 | 0.0010 | 0.0034 | 0.0018 | 0.0006 | 0.0186 |
| SE PA | 0.0021 | 0.0009 | 0.0007 | 0.0050 | 0.0007 | 0.0021 | 0.0016 | 0.0007 | 0.0009 | 0.0007 | 0.0013 | 0.0043 | 0.0031 | 0.0009 | 0.0251 |
| C PA | 0.0002 | 0.0013 | 0.0020 | 0.0075 | 0.0009 | 0.0031 | 0.0024 | 0.0010 | 0.0014 | 0.0010 | 0.0020 | 0.0073 | 0.0070 | 0.0017 | 0.0388 |
| W PA | 0.0000 | 0.0004 | 0.0033 | 0.0065 | 0.0011 | 0.0044 | 0.0035 | 0.0015 | 0.0021 | 0.0018 | 0.0033 | 0.0125 | 0.0195 | 0.0037 | 0.0635 |
| PA SEN A | 0.0001 | 0.0008 | 0.0019 | 0.0154 | 0.0017 | 0.0045 | 0.0028 | 0.0010 | 0.0012 | 0.0008 | 0.0023 | 0.0102 | 0.0052 | 0.0014 | 0.0492 |
| MD DC | 0.0002 | 0.0003 | 0.0007 | 0.0146 | 0.0017 | 0.0042 | 0.0022 | 0.0008 | 0.0008 | 0.0005 | 0.0017 | 0.0074 | 0.0023 | 0.0007 | 0.0383 |
| DE | 0.0004 | 0.0003 | 0.0004 | 0.0074 | 0.0011 | 0.0028 | 0.0016 | 0.0006 | 0.0007 | 0.0004 | 0.0012 | 0.0046 | 0.0017 | 0.0006 | 0.0237 |
| VA | 0.0000 | 0.0001 | 0.0005 | 0.0190 | 0.0028 | 0.0056 | 0.0027 | 0.0009 | 0.0008 | 0.0004 | 0.0020 | 0.0080 | 0.0015 | 0.0006 | 0.0448 |
| NE WV | 0.0000 | 0.0001 | 0.0011 | 0.0385 | 0.0057 | 0.0119 | 0.0049 | 0.0014 | 0.0013 | 0.0008 | 0.0042 | 0.0239 | 0.0033 | 0.0013 | 0.0983 |
| SW WV | 0.0000 | 0.0000 | 0.0003 | 0.0099 | 0.0071 | 0.0193 | 0.0074 | 0.0017 | 0.0013 | 0.0006 | 0.0061 | 0.0254 | 0.0014 | 0.0009 | 0.0814 |
| E KY | 0.0000 | 0.0000 | 0.0000 | 0.0039 | 0.0011 | 0.0268 | 0.0236 | 0.0035 | 0.0016 | 0.0006 | 0.0160 | 0.0163 | 0.0005 | 0.0005 | 0.0914 |
| W KY | 0.0000 | 0.0000 | 0.0000 | 0.0002 | 0.0001 | 0.0075 | 0.0541 | 0.0106 | 0.0013 | 0.0003 | 0.0134 | 0.0026 | 0.0001 | 0.0002 | 0.0904 |
| W TN | 0.0000 | 0.0000 | 0.0000 | 0.0001 | 0.0000 | 0.0014 | 0.0057 | 0.0053 | 0.0004 | 0.0001 | 0.0019 | 0.0006 | 0.0000 | 0.0000 | 0.0156 |
| E TN | 0.0000 | 0.0000 | 0.0000 | 0.0004 | 0.0003 | 0.0039 | 0.0060 | 0.0023 | 0.0005 | 0.0001 | 0.0029 | 0.0017 | 0.0001 | 0.0001 | 0.0184 |
| Smokies | 0.0000 | 0.0000 | 0.0000 | 0.0006 | 0.0004 | 0.0035 | 0.0044 | 0.0017 | 0.0005 | 0.0001 | 0.0023 | 0.0018 | 0.0002 | 0.0001 | 0.0156 |
| C NC | 0.0000 | 0.0000 | 0.0001 | 0.0026 | 0.0012 | 0.0030 | 0.0023 | 0.0009 | 0.0004 | 0.0002 | 0.0014 | 0.0024 | 0.0004 | 0.0002 | 0.0151 |
| E NC | 0.0000 | 0.0000 | 0.0001 | 0.0023 | 0.0006 | 0.0015 | 0.0012 | 0.0005 | 0.0003 | 0.0001 | 0.0007 | 0.0014 | 0.0003 | 0.0001 | 0.0092 |
| SC | 0.0000 | 0.0000 | 0.0000 | 0.0008 | 0.0003 | 0.0010 | 0.0011 | 0.0006 | 0.0002 | 0.0001 | 0.0006 | 0.0008 | 0.0001 | 0.0001 | 0.0057 |
| NW GA | 0.0000 | 0.0000 | 0.0000 | 0.0002 | 0.0001 | 0.0008 | 0.0015 | 0.0011 | 0.0002 | 0.0001 | 0.0007 | 0.0005 | 0.0001 | 0.0001 | 0.0056 |
| SE GA | 0.0000 | 0.0000 | 0.0000 | 0.0002 | 0.0001 | 0.0003 | 0.0004 | 0.0004 | 0.0001 | 0.0000 | 0.0002 | 0.0002 | 0.0000 | 0.0000 | 0.0019 |

# RELATIVE IMPORTANCE OF PRIMARY AND SECONDARY SULFATE

J. D. Shannon

---

The primary sulfate emission factor, the percentage of sulfur oxides emitted in the form of sulfate for various source types, has received considerable interest recently. The significance of the issue derives from mandated oil "backout" legislation--a required switch from oil combustion to coal combustion in many Northeastern electric utilities. While combustion of coal usually produces more sulfur oxide emissions than combustion of oil, particularly low-sulfur oil, the primary sulfate emission factor is higher for oil combustion: 1.5 to 2.0 % for coal vs. 3.0 to 13.4 % for oil, depending upon oil type and boiler characteristics.

Oil combustion in the Northeast for other than power generation and industrial uses is highly seasonal; much oil is required for space heating and thus primary sulfate emissions are highest in winter. Since the mechanisms involved in the production of secondary sulfate through atmospheric transformation of $SO_2$ are less effective in winter because of lower humidity, temperature, and solar intensity, the relative importance of primary sulfate is greater then.

The ASTRAP model has been modified to treat the primary sulfate emission factor as an input in calculations of concentrations and deposition. Assumed emission factors for various source categories are given in Table 1, along with the emission totals. Residual oil, which has the highest sulfate emission factor, is burned in area sources in the Northeast, leading to the high values for that region.

Simulations of primary and secondary $SO_4^=$ for both winter and summer, produced by combining the simulations of each category in Table 1, are shown in Figures 1-4. It can be seen that secondary $SO_4^=$ dominates over most of eastern North America, particularly during summer, but primary sulfate is of equal importance in urbanized areas of the Northeast during winter.

Table 1. Sulfate emission factors and sulfur oxide emission rates.

| Source category | Emission rate equivalent tons $SO_2$/day | | Sulfate emission factor, % |
|---|---|---|---|
| | Summer | Winter | |
| Coal point sources | 42,000 | 40,000 | 1.5 |
| Residual oil point sources | 4,000 | 4,000 | 7.0 |
| Distillate oil point sources | 6,800 | 6,800 | 3.0 |
| Northeastern area sources | 4,500 | 9,600 | 13.4 |
| Southwestern area sources | 19,300 | 27,300 | 3.0 |

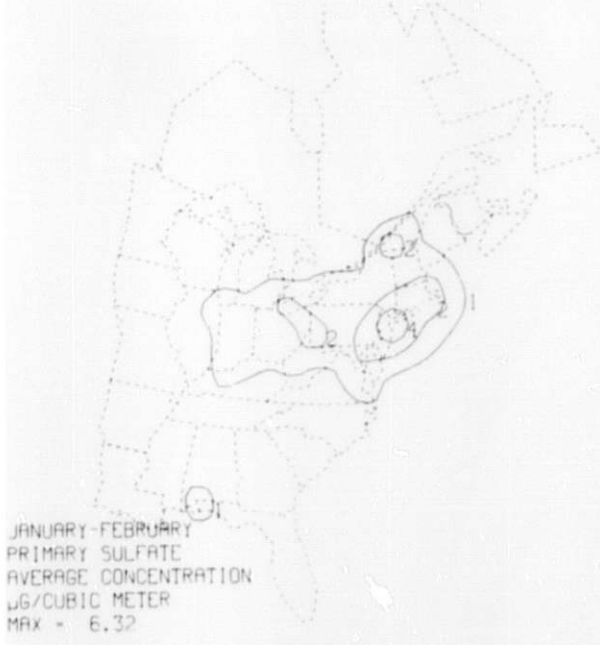


FIG. 1. Simulation of primary sulfate during winter.

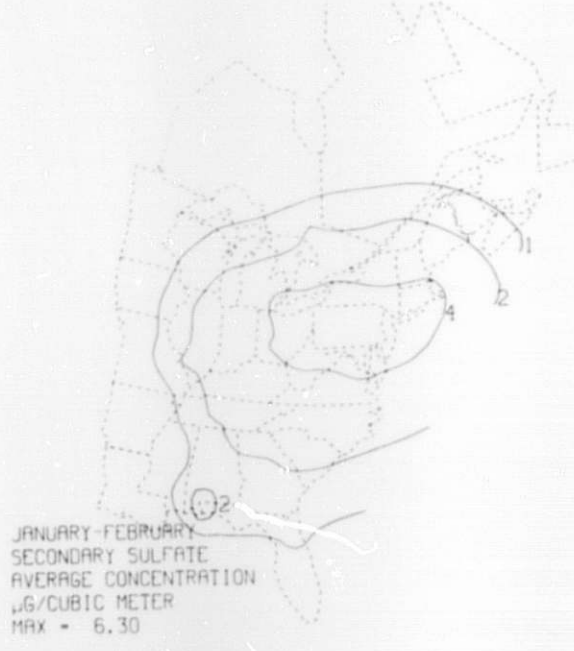


FIG. 2. Simulation of secondary sulfate during winter.


FIG. 3. Simulation of primary sulfate during summer.


FIG. 4. Simulation of secondary sulfate during summer.

# SIMULATION OF THE EFFECTS OF FUEL CONVERSION IN THE NORTHEAST

J. D. Shannon

A major component of the Federal plan to reduce oil imports is the conversion of 42 oil-burning power plants in the Northeast to coal combustion. This implies many changes in the mix of pollution emissions. A switch to coal will generally result in greater emissions of sulfur oxides, since low-sulfur oil is currently used in almost every plant. On the other hand, coal has a lower primary sulfate emission factor (fraction) than oil; thus, for some sources the sulfate emitted directly may be reduced after conversion. In some cases, plants being converted and expanded will have taller stacks, which shift the deposition process further downstream. In other cases, installation of improved pollution controls during conversion will reduce total emissions.

For simulation of regional patterns of average concentrations arising from multiple sources and regional patterns of deposition, a long-range transport model must be used. The ASTRAP model (Shannon, 1981) has been used for such purposes as part of a regional environmental impact study with the results highlighted below.

The coastal location of nearly all the candidate plants leads to transportation of the bulk of emitted sulfur oxides ( $\approx$ 85%) out to sea before deposition, whether wet or dry. Thus, the increment of wet or dry deposition in areas of the Northeast is less than might be expected from the magnitude of the emission increase (Table 1). The largest percentage increase shown (Nova Scotia) follows from the facts that Nova Scotia is downwind (northeast) of the sources much of the time and that the base-case simulations of anthropogenic sulfur concentrations and deposition are quite low there.

A graphic presentation of simulation of a particular case is given in Figure 1, along with budget figures. The dominance of transport out to sea (emissions minus continental deposition) is clearly seen.

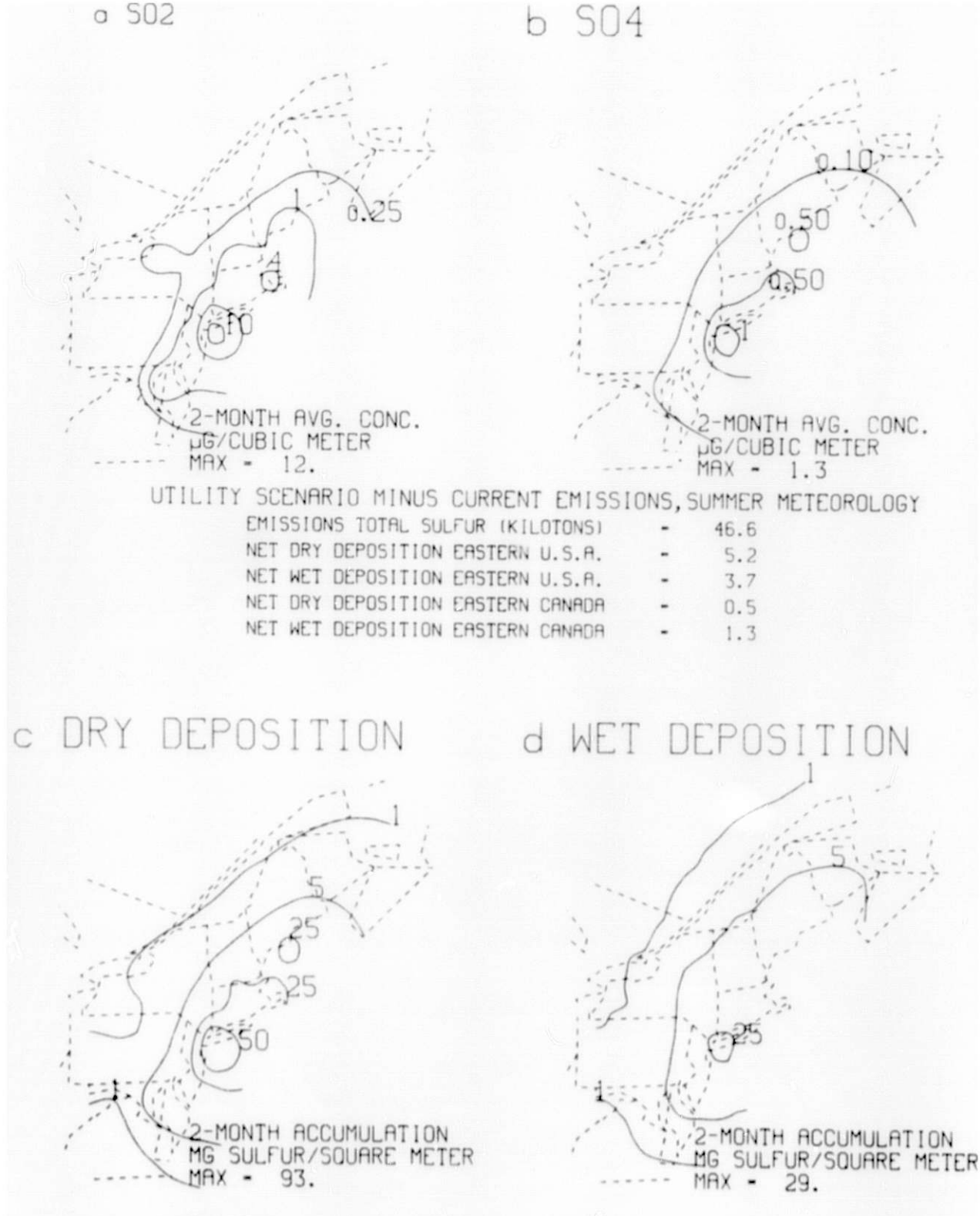


FIG. 1. Incremental effects of fuel conversion during two summer months.

Table 1. Incremental effects of utility emissions, July-August meteorology.

| | E. North America base case | Utility Scenario increase |
|---|---|---|
| Emissions, kT S | 2240 | 46.6 |
| Wet Deposition U.S., kT S | 675 | 3.7 |
| Wet Deposition Canada, kT S | 235 | 1.3 |
| Dry Deposition U.S., kT S | 490 | 5.2 |
| Dry Deposition Canada, kT S | 110 | 0.5 |
| Wet Deposition Adirondacks, g S $m^{-2}$ | 0.300 | 0.005 |
| Wet Deposition Nova Scotia, g S $m^{-3}$ | 0.080 | 0.005 |
| $SO_4^=$ Concentration Adirondacks, μg $m^{-3}$ | 6.0 | 0.10 |
| $SO_4^=$ Concentration Nova Scotia, μg $m^{-3}$ | 2.5 | 0.12 |

Reference

Shannon, J. D., 1981: A model of regional long-term average sulfur atmospheric pollution, surface removal, and net horizontal flux, Atmos. Environ. 15, 689-701.

# PRELIMINARY MODELING OF REGIONAL $NO_x$/NITRATE CONCENTRATIONS AND DEPOSITION

J. D. Shannon

---

While there is general awareness that chemical deposition is a witch's broth of various ions, numerical modelers of long-range transport and deposition have used deposition of total sulfur as a surrogate for the overall process; pollutant sulfur appears to be the most important contributor to precipitation acidity. Experimental results indicate that nitrate is also an important chemical constituent (Dana, 1980). Nitrogen chemistry has been studied extensively in smog chambers and in urban areas, particularly on the west coast, but investigation of removal mechanisms and transport of pollutant nitrogen on the regional scale has been very limited. Some preliminary measurements of dry deposition of $NO_x$ have been made (Wesely et al., 1981), but dry deposition of nitrate, as nitric acid or otherwise, remains an unresolved issue.

If linear first-order chemistry is an acceptable approximation in regional-scale transformation of $NO_x$ to nitrate, and if parameterization of wet removal of pollutant nitrogen as a bulk removal coefficient proportional to the precipitation amount raised to some power is acceptable, then the ASTRAP model (Shannon, 1981) can be used to simulate long-term average regional patterns of nitrogen pollutants. In other words, while the average values and the diurnal and seasonal variations of transformation and removal rates suggested by parameterizations can be different for the pollutant sulfur and pollutant nitrogen systems, the methods of calculation can be identical.

Some preliminary simulations, in which the values of the $NO_x$/nitrate modeling parameterizations are as follows,

Dry Deposition: Diurnal and seasonal variation in deposition velocities
summer average 0.42 cm $s^{-1}$ ($NO_x$), 0.93 cm $s^{-1}$ ($NO_3^-$)
ranges 0.08 to 0.85 cm $s^{-1}$ ($NO_x$), 0.2 to 1.7 cm $s^{-1}$ ($NO_3^-$).

Transformations: Diurnal and seasonal variation;
summer average $NO_x \rightarrow NO_3^-$ 4% $hr^{-1}$; range 0.2 to 12% $hr^{-1}$.

Wet Removal: Bulk removal coefficient $R = (h/10)^{1/2}$, where h is the precipitation in mm per 6 hours.

Primary Nitrate: Optional - zero in example shown.

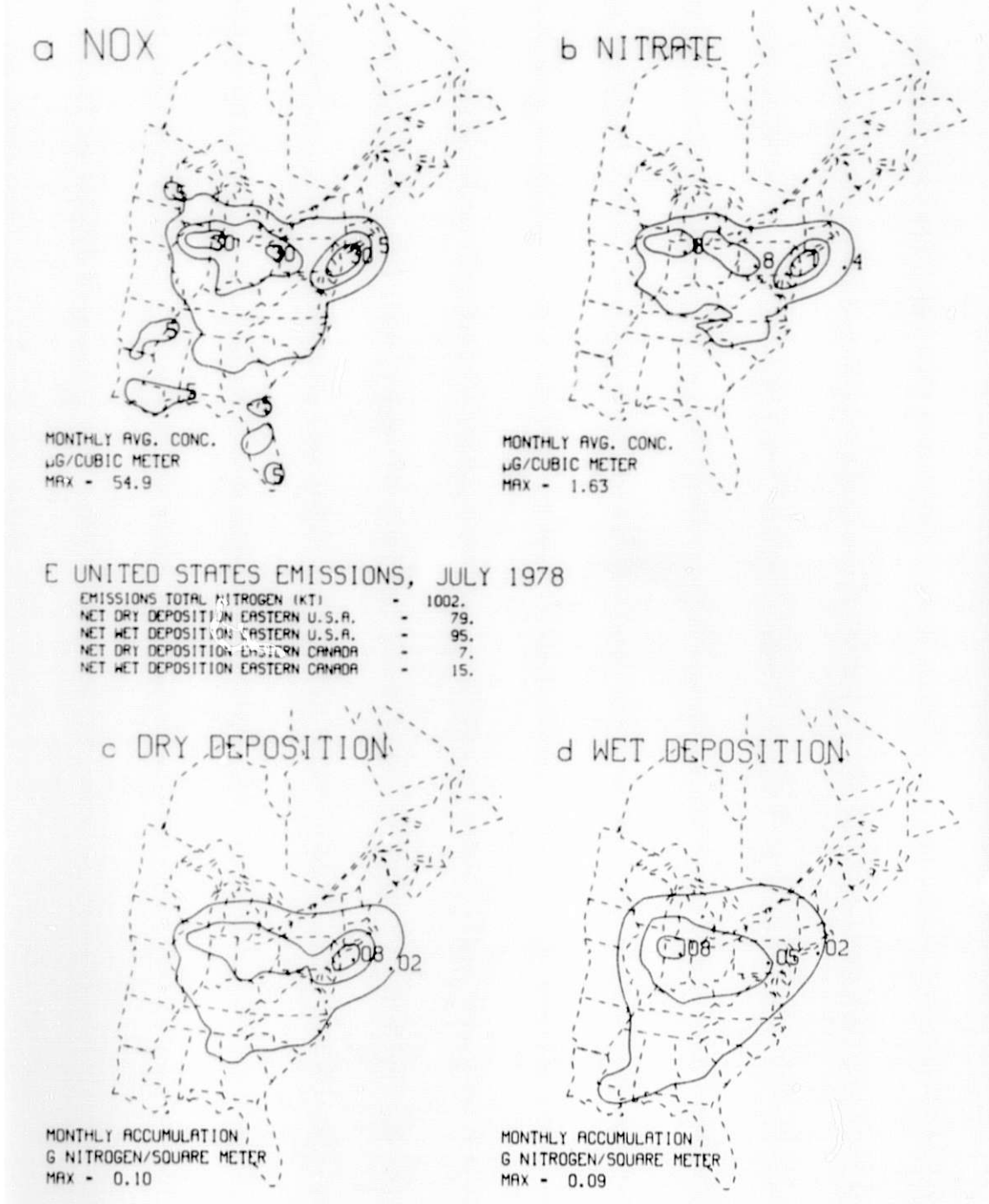


FIG. 1. Simulation of pollutant nitrogen concentrations and deposition.

are contoured in Figure 1. The emissions are as given in the MAP3S emission inventory. The more rapid dry deposition of nitrate, the relatively fast $NO_x$ to nitrate conversion, and the concentration of sources in urban areas because of gasoline combustion combine to create maxima more oriented toward urban populations than is the case for pollutant sulfur, which is produced primarily by electric power generation in nonurban areas.

References

Dana, M. T. Ed., 1980: The MAP3S precipitation chemistry network: Third periodic summary report (July 1978 - December 1979), Battelle Pacific Northwest Laboratory.

Shannon, J. D., 1981: A model of regional long-term average sulfur atmospheric pollution, surface removal, and net horizontal flux, Atmos. Environ. 15, 689-701.

Wesely, M. L., J. A. Eastman, D. H. Stedman, and E. D. Yalvac, 1981: An eddy-correlation measurement of $NO_2$ flux to vegetation and comparison to $O_3$ flux, Atmos. Environ., in press.

# ANALYSIS OF PRECIPITATION DATA FOR USE IN ASTRAP

J. D. Shannon

Precipitation data are routinely archived by the National Weather Service in the form of a series of hourly values for a year for each station, one magnetic tape for each station. This form is convenient if the statistics of precipitation amount and frequency at a single station are being analyzed, but is awkward when a time series of spatial objective analyses must be performed, since the required data are stored on many different magnetic tapes. Fortunately, precipitation data for several meteorological periods of interest, including Canadian data, have been organized in synoptic form (i.e., all reporting stations for each time period) by a consultant for EPA. Then, the task remaining before use in ASTRAP is to analyze a time series of fields of 6-hr precipitation for eastern North America.

Summing the hourly observations for six consecutive hours is a simple initial step. The method of transferring the information at irregularly-spaced observation sites to a regularly-spaced analysis grid requires more thought. In the associated matter of analyses of wind fields, wind speed and direction are transformed to u and v components. The components are continuous in distribution and vary relatively smoothly across the region; an inverse-distance-squared weighting scheme produces satisfactory analyses. Precipitation, on the other hand, has a Poisson distribution; negative values cannot occur and the most common observation is zero. An inverse distance-squared weighting would cause the analysis to show rainfall more frequent and less in amount for each event than occurs in nature, since weighting of zero and nonzero values will produce a nonzero value in every case.

The method selected here is to assign to each gridpoint the closest observation. This method has a separate problem in that the gridpoints around the only station in a data-sparse area, such as northern Ontario, will all have the same value, However, the precipitation amount and frequency is unbiased.

Four consecutive analyses produced by this method are shown in Figure 1. The analysis is for a grid spacing of about 65 km. The nonzero values of the analysis can be seen to progress, although not nearly as smoothly as in classical meteorology.

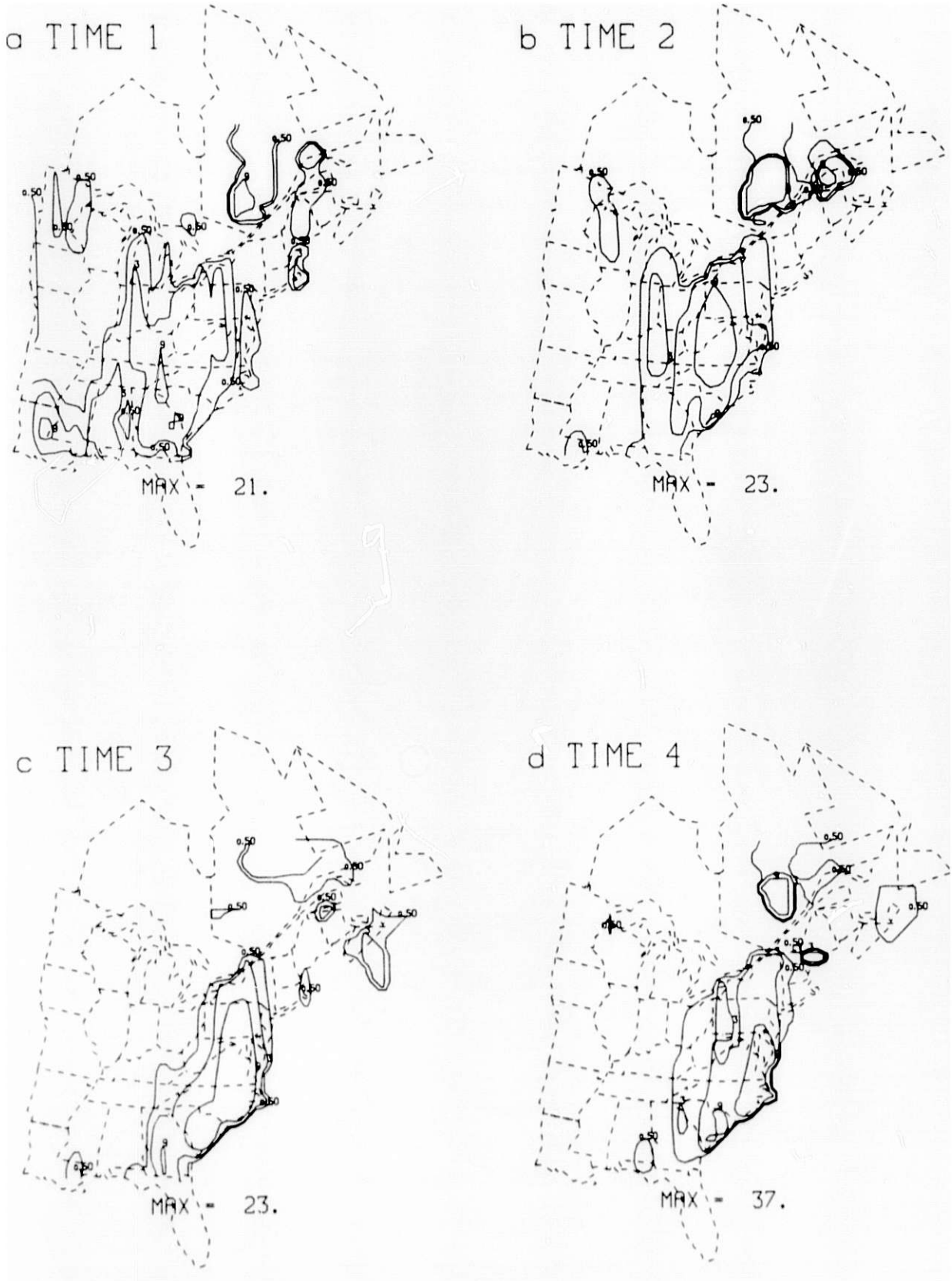


FIG. 1. Example of ASTRAP precipitation preprocessing for July 14, 1978 (0000 to 1800 GMT)

# SIMULATION OF POLLUTANT DIURNAL VARIATIONS IN THE LOWER ATMOSPHERE

I. Y. Lee and T. Yamada

---

A one-dimensional model simulating the diurnal variation of pollutants in the lower atmosphere combines atmospheric variables produced by a second-moment turbulence-closure model (Yamada, 1978) with a chemical kinetics model (Swan and Lee, 1980). While pollutant concentrations depend on initial concentrations, sources, vertical mixing, surface deposition, solar activity, advection and chemical reactions, the kinetics model currently includes only homogeneous reactions, and the contributions due to advection and local sources are not considered.

The deposition velocity is computed as suggested by Wesely and Hicks (1977). Simulated temporal and spatial variations of eddy diffusivity (Figure 1) are used together with input surface variables in agreement with measurements (Figure 2) from the Sangamon experiment of July 1975. The initial concentrations for most of the chemical species are taken from reports in the literature; the initial ozone and sulfur dioxide concentrations are assumed to be the nighttime background values observed at Argonne.

The variations of singlet oxygen due to photochemistry (Figure 3) exhibits a peak value of 1.7 ppq at 1200 CST. The concentrations of NO, $HNO_2$, and OH increase to their maxima of 7 ppb at 0700, 0.15 ppb at 0800 and 45 ppq at 1000 CST, respectively. On the other hand, $NO_2$ (~ 30 ppb) and $H_2O_2$ (~ 20 ppb) decrease slowly, by about 10 percent during the 8-hr simulation. The concentration patterns for $O_3$, $NO_3$, $N_2O_5$, $HNO_3$ and $HO_2$ are generally similar, with that for $O_3$ shown in Figure 4 being representative of the five. Here we see the gradual formation of the concentration jump near the top of the mixed layer; surface deposition is responsible for the lower concentrations in the mixed layer and in the surface layer. The time evolution of $O_3$, NO, $NO_2$, and F, the apparent conversion factor between ozone and nitrogen oxides, indicates that F is very close (within ± 5%) to the photostationary value (Figure 5), and that the photochemical production of ozone can be determined as a steady-state value, if advection and local emissions of nitrogen oxides are negligible. Finally, the ozone concentrations simulated with different initial $NO_2$/NO ratios compare favorably with observations made at Argonne National Laboratory (Figure 6).

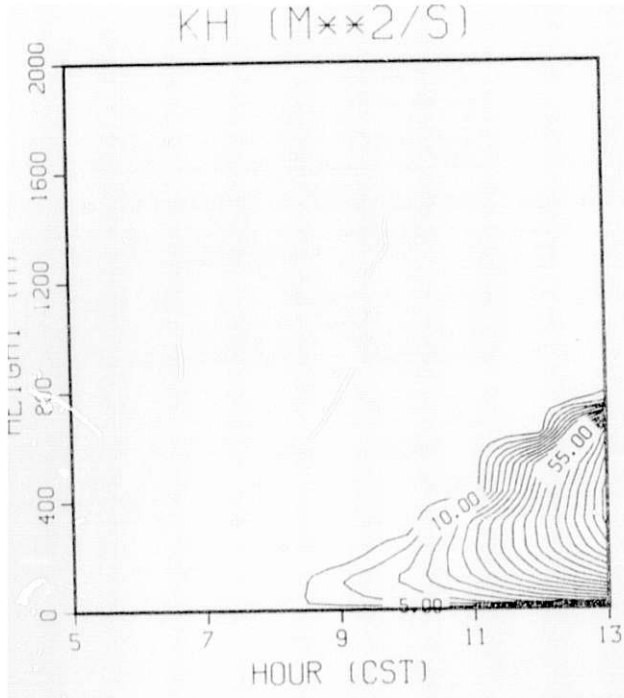


FIG. 1. Temporal and spatial variations of the computed eddy diffusion coefficients.

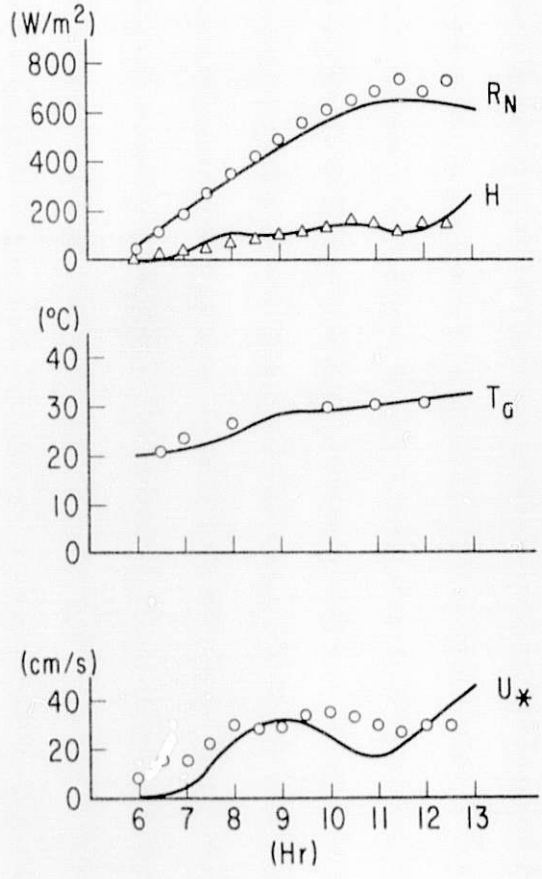


FIG. 2. Comparison of the computed (solid line) and observed (symbols) values of surface variables: $R_N$, net radiation; H, sensible heat flux; $T_a$, air temperature; $U_*$, friction velocity.

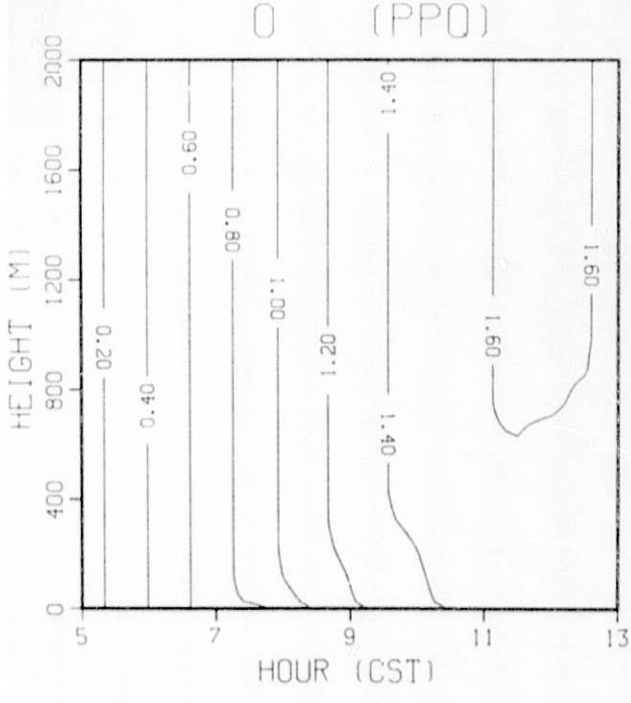


FIG. 3. Temporal and spatial variations of singlet oxygen.

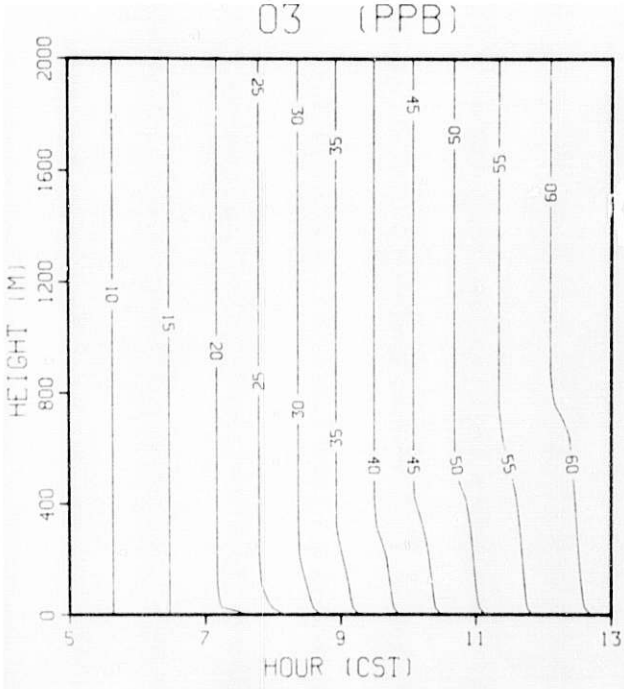


FIG. 4. Temporal and spatial variations of ozone.

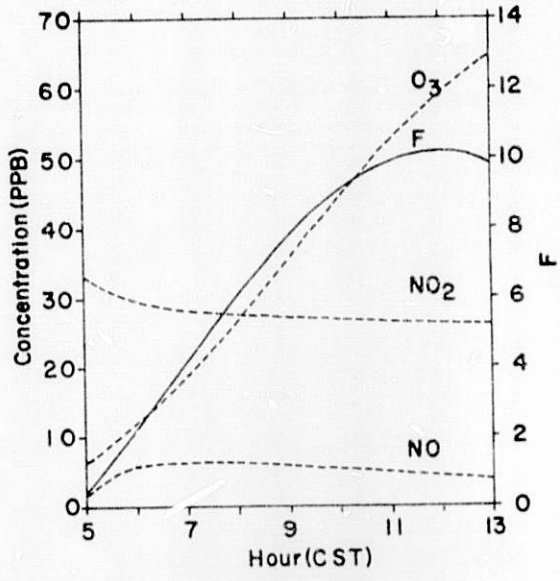


FIG. 5. Profiles of $O_3$, $NO_2$, NO and the conversion factor F. $O = NO_2/NO$.

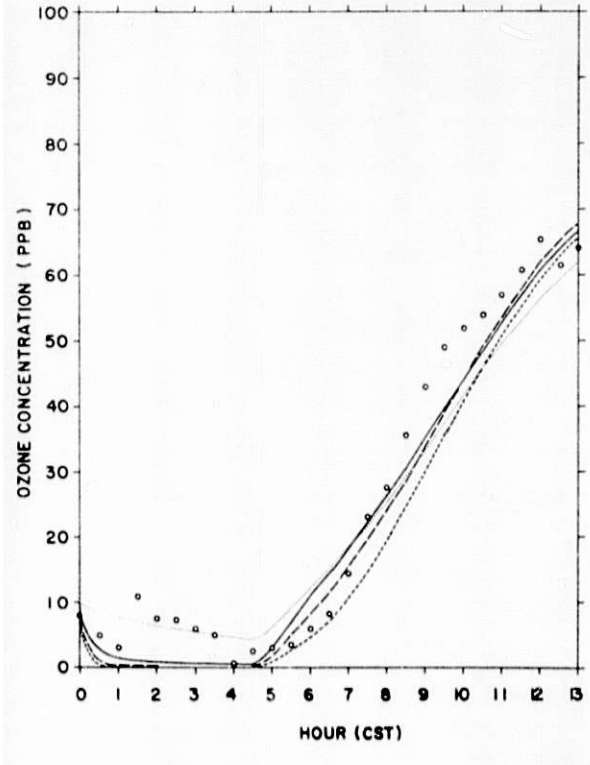


FIG. 6. Comparison of the computed and observed values of ozone at 7.6 m above the ground. Observed, 0; computed for initial $R = NO/NO_2$ = 0.025, ....; = 0.25, --; = 0.50, ---; = 1.00, ----.

While this report is preliminary in nature, the combination of detailed meteorology and air chemistry appears profitable for understanding the behavior of pollutants in the lower atmosphere. Further development of the model, in progress, will include heterogeneous processes and conservation equations associated with the reactions of various hydrocarbons.

## References

Swan, P. R. and I. Y. Lee, 1980: Meteorological and air pollution modeling for an urban airport, J. Appl. Meteorol. 19, 534-544.

Wesely, M. L. and B. B. Hicks, 1977: Some factors that affect the deposition rates of sulfur dioxide and similar gases on vegetation, J. Air Pollut. Control Assoc. 27, 1110-1116.

Yamada, T., 1978: A three-dimensional, second-order closure numerical model of mesoscale circulations in the lower atmosphere, Argonne National Laboratory report ANL/RER-78-1.

# HOMOGENEOUS GAS KINETICS MODEL

I. Y. Lee

Swan and Lee (1980) developed a chemical kinetics model to simulate homogeneous reactions in the atmosphere. The 23 reactions involving 19 chemical species (Swan and Lee, Table 1) are quite cumbersome computationally, partially because the rate equations describing photochemistry involve time constants << 1 s; without simplication, only implicit techniques can be used to solve the large set of equations (which are linearized for computational purposes) during temporal integration. The model has now been modified to increase efficiency without significant loss of accuracy. First, a partitioning procedure takes advantage of the fact that some species do not involve time constants that are short compared to desired integration time steps, and thus their concentration equations can be integrated explicitly. The remainder are integrated with an implicit technique, but the reduced number of species in the latter category decreases computation time significantly. A pulse technique is used to determine the time constants involved in the concentration of each species. This method, which can produce a graphical depiction of the significant time constants for each variable, consists of carrying out a "baseline" integration of the kinetics in order to obtain a set of initial conditions. Subsequent integrations differ only in that the initial concentration of each species, in turn, is perturbed slightly from its baseline value. For each such integration, a plot of the evolving concentration against the log of the integration time reveals a typical exponential decay at the rate involved in the evolution of that species. The results of such an analysis for three selected species are shown in Figure 1, and indicate three typical kinds of behavior: the atomic oxygen concentration reacts very rapidly with a time constant of slightly over 10 μs (at the 1/e point of the left-hand curve); $NO_3$ changes with two time constants, one of ~ 0.25 s and one of ~ 26 s; CO evolves with a time contant of almost 35,000 s. This partitioning technique results in eleven variables (O, $O_3$, $NO_2$, $NO_3$, $N_2O_5$, OH, $HO_2$, $SO_3$, $HSO_3$, and $H_2SO_4$) being integrated implicitly, and six ($HNO_2$, $HNO_3$, $H_2O_2$, $SO_2$, CO and $CO_2$) explicitly. Two species ($H_2O$ and $O_2$) are not integrated at all, since their concentrations do not change perceptibly as a result of chemical reactions.

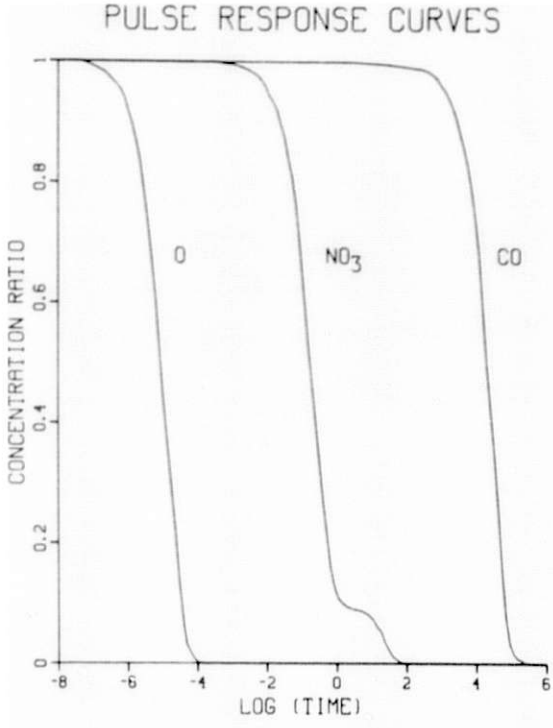


FIG. 1. Pulse response of chemical kinetics model to determine time constants of O, $NO_3$, and CO.

The second modification to increase computational efficiency involves computer-generated subroutine codes used for the solution of the equations. These optimal codes no not use loop coding, and avoid all operations on zeros in the computation. Thus, only nonzero elements of the Jacobian of the implicit partition are calculated, and only nonzero operations are performed to solve the linear set of equations. Because of the extreme sparseness of the array of coefficients defining the linear equation set, the avoidance of computer operations on the zero terms leads to a sizable reduction in overall computational cost.

Comparisons with fully implicit integrations of the entire set of 19 species demonstrate that the errors involved in the partitioning are less than one percent over an integration time of 24 hr. Implementation of these two techniques reduces computation time to about 2 ms per grid point per time step on an IBM 370/195 computer, one order of magnitude faster than an implicit solution for 19 species with standard coding.

## Reference

Swan, P. R., and I. Y Lee, 1980: Meteorological and air pollution modeling for an urban airport. J. Appl. Meteorol., 19, 534-544.

# RESULTS OF THE 1980 RAIN CHEMISTRY ROUND ROBIN

D. L. Sisterson

In February 1980, approximately 25 chemistry laboratories participated in a rain chemistry round robin sponsored by the Environmental Protection Agency (EPA). The results to date have not been distributed to the participants. While the ANL rain chemistry program was not fully operational at that time, the Analytical Chemistry Laboratory (ACL) at ANL analyzed the same blind samples late in December 1980. The ACL results are compared below to those from the Central Analytical Laboratory (CAL) at the Illinois State Water Survey, the Environmental Monitoring Laboratory (EML) and Rockwell International (RI). These laboratories were chosen since they are all highly qualified in rain chemistry analysis and are all actively involved in analyzing rain samples for major networks. CAL analyzes weekly rain samples for the National Atmospheric Deposition Program network, EML analyzes monthly rain samples for the World Meteorological Organization network, and RI analyzes rain samples for the Electric Power Research Institute Sulphur Regional Experiment network.

The rain simulant samples furnished by the EPA in the 910000 and 920000 series ampoules are chemically concentrated. When diluted to 500 ml, they simulate typical low and high concentrations of environmental pollutants found in rainwater samples. The analytical methods employed by the laboratories for each ion are given in Table 1. Table 2 summarizes the results of the rain chemistry round robin. The values of $Ca^{++}$ reported by EML are roughly a factor of 2 lower than those of the other laboratories; since the ML values were independently verified, the ampoules concentrations of $Ca^{++}$ are suspect.

Ion concentration averages and standard deviations for the laboratory analyses (EML $[Ca^{++}]$ values are not included) demonstrate excellent agreement among the laboratories and with EPA. The largest differences among the individual laboratories are in pH values in the 910000 series and in $[Cl^{-}]$ in the 920000 series ampoules; the major differences between the laboratory averages and EPA are in pH and $[Na^{+}]$ in the 910000 series and pH and $[Cl^{-}]$ in the 920000 series ampoules.

Table 1. Analytical methods used for each of the four laboratories.

| Ion | ACL | CAL | EML | RI |
|---|---|---|---|---|
| $SO_4^{=}$ | IC | IC | IC | IC |
| $NH_3^{-}$ | IC | AA | AA | AA |
| $NO_3^{-}$ | IC | AA | IC | IC |
| $Cl^{-}$ | IC | AA | IC | IC |
| $F^{-}$ | IC | SIE | IC | IC |
| $Ca^{++}$ | FAA | FAA | FAA | FAA |
| $K^{+}$ | IC | FAA | FAA | FAA |
| $Mg^{++}$ | FAA | FAA | FAA | FAA |
| $Na^{+}$ | IC | FAA | FAA | FAA |

IC = Ion chromatograph; AA = Auto analyzer;
SIE = Selective ion electrode; FAA = Flame atomic absorption

Table 2. Results of rain chemistry round robin in mg $L^{-1}$.

910000 Series Ampoule

| | ACL | CAL | EML | RI | 4 Laboratory Average | σ | EPA |
|---|---|---|---|---|---|---|---|
| pH | 4.94 | 5.06 | ---- | 4.83 | 4.94 | 0.12 | 5.03 |
| $SO_4^{=}$ | 0.32 | 0.28 | 0.263 | 0.253 | 0.28 | 0.03 | 0.260 |
| $NH_3^{+}$ | 0.19 | 0.17 | 0.162 | 0.178 | 0.18 | 0.01 | 0.166 |
| $NO_3^{-}$ | 0.19 | 0.19 | 0.187 | 0.193 | 0.19 | - | 0.186 |
| $Cl^{-}$ | 0.89 | 0.98 | 0.826 | 0.868 | 0.89 | 0.07 | 0.908 |
| $F^{-}$ | 0.17 | 0.14 | 0.147 | 0.164 | 0.16 | 0.01 | 0.154 |
| $Ca^{++}$ | 0.23 | 0.24 | 0.131* | 0.239 | 0.24 | 0.01 | 0.248 |
| $K^{+}$ | 0.13 | 0.146 | 0.159 | 0.269 | 0.18 | 0.06 | 0.156 |
| $Mg^{++}$ | 0.06 | 0.056 | 0.062 | 0.056 | 0.06 | - | 0.056 |
| $Na^{+}$ | 0.32 | 0.282 | 0.300 | 0.313 | 0.30 | 0.02 | 0.284 |

920000 Series Ampoule

| | | | | | | | |
|---|---|---|---|---|---|---|---|
| pH | 4.31 | 4.28 | ---- | 4.18 | 4.26 | 0.07 | 4.35 |
| $SO_4^{=}$ | 0.81 | 0.91 | 0.752 | 0.776 | 0.81 | 0.07 | 0.776 |
| $NH_3^{+}$ | 0.58 | 0.54 | 0.547 | 0.537 | 0.55 | 0.02 | 0.514 |
| $NO_3^{-}$ | 0.51 | 0.49 | 0.482 | 0.493 | 0.49 | 0.01 | 0.485 |
| $Cl^{-}$ | 0.24 | 0.29 | 2.81 | 3.46 | 3.20 | 0.28 | 0.274 |
| $F^{-}$ | 0.27 | 0.24 | 0.255 | 0.338 | 0.28 | 0.04 | 0.256 |
| $Ca^{++}$ | 0.64 | 0.67 | 0.363* | 0.646 | 0.65 | 0.02 | 0.654 |
| $K^{+}$ | 0.48 | 0.488 | 0.520 | 0.513 | 0.50 | 0.02 | 0.506 |
| $Mg^{++}$ | 0.24 | 0.230 | 0.237 | 0.223 | 0.23 | 0.01 | 0.226 |
| $Na^{+}$ | 0.62 | 0.542 | 0.570 | 0.591 | 0.58 | 0.03 | 0.558 |

*Vales not used in 4-laboratory average.

While this is ACL's first participation in a rain chemistry round-robin, the results clearly demonstrate ACL's ability to analyze precipitation samples accurately.

Acknowledgements

Don Bogen (EML), Mark Penden (CAL), and Leo Topol (RI) provided the data for this report and their cooperation is appreciated.

# A COMPARISON OF THE ACIDITY OF EVENT AND WEEKLY PRECIPITATION SAMPLES IN NORTHERN ILLINOIS -- A PRELIMINARY REPORT, PART I.

D. L. Sisterson and B. Wurfel†

Argonne National Laboratory is a designated collection site for the National Atmospheric Deposition Program (NADP) and conducts related research for the Multistate Atmospheric Power Production Pollution Study (MAP3S). The NADP network collects weekly precipitation samples to monitor rainfall quality with emphasis on those properties that could have potentially adverse effects on ecological and agricultural systems. The MAP3S program focuses on event sampling in order to investigate the mechanisms whereby pollutants are scavenged by precipitation. This preliminary report examines the differences between the weekly sums of event samples weighted by event precipitation amount (these samples are designated ANL samples) and the corresponding NADP weekly samples for pH and conductivity and total, strong, and weak acid concentrations. The chemical analysis of these samples is discussed in another report (Sisterson and Wagner, 1980). The results of the acidity and chemical analyses will help determine whether weekly and event precipitation network data can be combined in a realistic manner.

Since April 1980, two Aerochem Metrics automatic wet/dry precipitation collectors placed approximately 5 m apart have been activated by a single sensor at Argonne's open, grassy collection site, which is free from large trees and other obstacles for at least 50 m in all directions. The site is located 400 m away from a lightly traveled roadway and approximately 30 km north and northwest of several large refineries and a coal-burning power plant. Event samples were removed from the collector and frozen after each rain event during the day. When precipitation occurred at night, the samples were removed as soon as possible the following morning. In some cases, rain samples collected during the weekend were not removed from the collector until Monday morning. On several occasions, more than one precipitation event was collected in the event bucket; for this study, they were regarded as a single

† Student Aide (May-August and December 1980). Present affiliation: Beloit College, Beloit, Wisconsin.

event. Weekly samples were removed from the collectors each Tuesday morning, as specified by NADP operating procedures.

The acidity analysis was performed by removing 50 ml aliquots from both NADP and event samples. After samples came to room temperature (~ 20 °C), pH and conductivity were measured, and titrations according to a procedure outlined by Gran (1952) were performed. Conductivity and pH measurements were made using a Markson Digital Electromark Analyzer pH meter in conjunction with a Beckman Futura*, refillable, combination pH electrode and a Markson* conductivity cell. The titration procedures and pH measurements are described elsewhere (Irving, 1978; Sisterson and Irving, 1979).

Data for ANL and NADP samples for 33 weeks are presented in Table 1. Rigorous tests of statistical significance are in progress, but preliminary findings of the comparison of ANL and NADP data summed over the entire 33-week study period are included in Table 2. The ANL samples have more strong acids present and more dissociated hydrogen ions than NADP samples. The 33-week weighted ANL pH value was 4.19; that of NADP was 4.27. It is suggested that strong acids deposited in the precipitation are chemically altered during the time the NADP sample remains in the bucket prior to weekly collection. Several explanations are possible. The mixing of two or more precipitation samples may not be additive. Also, because the collection buckets are very large (13 L capacity), only a very small percentage of the bucket is filled even after the heaviest of rains. A large surface area of the sample is exposed to the air trapped in the bucket after the collector is closed. Enhanced exchange of volatile species between the sample and head space seems likely (Sisterson and Tisue, 1979). Futhermore, dirt and dust particles, insect parts and other organic material that contribute to bacteriological activity (particularly during the warmer months) may aid neutralization of the strong acids.

* No endorsement by Argonne is implied.

Table 1. Acidity analysis of weekly summed event (ANL) and weekly (NADP) precipitation samples.

| Sample | | Date 1980 | | pH | | $[H^+]x10^{-5}l^{-1}$ | | Conductivity μΩ ohm | | TAC | | SAC | | WAC | |
|---|---|---|---|---|---|---|---|---|---|---|---|---|---|---|---|
| | | | | | | | | | | | | x $10^{-4}$ eq $l^{-1}$ | | | |
| ANL | NADP | ANL | NADP | ANL | NADP | ANL | NADP | ANL | NADP | ANL | NADP | ANL | NADP | ANL | NADP |
| 4 | | 4/8 | | 4.03 | 4.08 | .933 | .832 | 53.8 | 55.5 | 2.430 | 2.740 | 1.940 | 1.040 | 1.580 | 1.700 |
| 5 | | 4/15 | | | | | | CM | | | | | | | |
| 6 | | 4/22 | | | | | | NP | | | | | | | |
| 7 | | 4/29 | | | | | | CM | | | | | | | |
| 8 | | 5/6 | | | | | | NP | | | | | | | |
| 9 | | 5/13 | | 4.34 | 4.25 | .457 | .562 | 34.3 | 37.2 | 1.581 | 1.606 | .522 | .612 | 1.059 | .994 |
| 10 | | 5/20 | | 4.20 | 4.26 | .630 | .549 | 56.0 | 20.1 | 1.518 | 2.023 | .666 | .606 | .852 | 1.417 |
| 11 | | 5/27 | | | | | | IS | | | | | | | |
| 12 | | 6/3 | | 4.30 | 4.41 | .501 | .389 | 29.6 | 25.7 | 2.229 | 2.199 | .598 | .439 | 1.610 | 1.760 |
| 13 | | 6/10 | | 4.39 | 4.88 | .407 | .132 | 26.9 | 19.9 | 2.011 | 2.528 | .466 | .210 | 1.121 | 2.318 |
| 14 | | 6/17 | | 4.18 | 4.21 | .661 | .616 | 43.9 | 49.2 | 2.109 | 3.088 | .638 | .531 | 1.471 | 2.557 |
| 15 | | 6/24 | | 4.31 | 4.49 | .490 | .324 | 39.5 | 25.4 | 2.432 | 2.505 | .522 | .325 | 1.910 | 2.180 |
| 16 | | 7/1 | | 3.96 | 4.03 | 1.096 | .933 | 57.7 | 49.7 | 3.004 | 2.474 | .926 | .788 | 2.078 | 1.684 |
| 17 | | 7/8 | | 4.37 | 4.68 | .426 | .209 | 5.01 | 36.6 | 2.914 | 2.992 | .487 | .283 | 2.427 | 2.709 |
| 18 | | 7/15 | | 4.26 | 4.37 | .549 | .426 | 29.2 | 22.7 | 1.553 | 1.254 | .615 | .398 | .938 | .856 |
| 19 | | 7/22 | | 4.04 | 4.11 | .912 | .776 | 48.6 | 40.8 | 2.738 | 2.374 | 1.210 | .801 | 1.529 | 1.573 |
| 20 | | 7/29 | | EM | | | | 70.0 | 65.9 | | | EM | | | |
| 21 | | 8/5 | | 4.33 | 4.50 | .468 | .316 | 36.8 | 22.2 | 1.456 | 1.440 | .558 | .366 | .898 | 1.074 |
| 22 | | 8/12 | | 4.07 | 4.58 | .851 | .263 | 37.1 | 36.8 | 2.025 | 2.005 | .916 | .283 | 1.109 | 1.722 |
| 23 | | 8/19 | | 4.10 | 4.14 | .794 | .724 | 57.8 | 39.3 | 1.794 | 1.655 | .911 | .772 | .883 | .883 |
| 24 | | 8/26 | | 4.03 | 4.11 | .933 | .776 | 43.6 | 36.1 | 2.328 | 1.416 | 1.080 | .768 | 1.248 | .648 |
| 25 | | 9/2 | | 4.23 | 4.26 | .589 | .549 | 27.2 | 27.3 | 1.890 | 1.353 | .501 | .553 | 1.389 | .800 |
| 26 | | 9/9 | | 4.25 | 4.30 | .549 | .501 | 27.7 | 28.8 | 1.718 | 1.394 | .642 | .827 | 1.076 | .827 |
| 27 | | 9/16 | | | | | | SC | | | | | | | |
| 28 | | 9/23 | | 4.58 | 4.61 | .263 | .245 | 14.6 | 16.6 | 1.045 | 1.353 | .263 | .229 | .781 | 1.124 |
| 29 | | 9/30 | | | | | | IS | | | | | | | |
| 30 | | 10/7 | | 6.36 | 6.55 | .004 | .003 | 15.2 | 20.9 | | | NT | | | |
| 31 | | 10/14 | | 4.78 | 4.78 | .166 | .166 | 20.6 | 21.0 | 1.166 | 1.178 | .211 | .197 | .955 | .981 |
| 32 | | 10/21 | | | | | | CM | | | | | | | |
| 33 | | 12/28 | | 4.36 | 4.37 | .436 | .426 | 26.8 | 258.2 | 1.554 | 1.585 | .467 | .490 | 1.087 | 1.095 |

$[H^+]$ is the hydrogen ion concentration and TAC, SAC, and WAC are the total, strong, and weak acid concentrations, respectively. CM is collector malfunction, NP is no precipitation, IS is insufficient sample for analysis, EM is electrode malfunction, NT is no titration, and SC is sample contamination.

Table 2. Acidity analysis of 33-week summed event (ANL) and summed weekly (NADP) precipitation samples. $[H^+]$ is the hydrogen ion concentration and TAC, SAC, and WAC are the total, strong, and weak acid concentrations, respectively. Percent difference is defined as the difference between the values (NADP-ANL) divided by the mean of the values.

| | | | $\times 10^{-4}$ equivalents | | |
|---|---|---|---|---|---|
| | $[H^+] \times 10^{-5}$ | Conductivity, $\mu\Omega$ | TAC | SAC | WAC |
| ANL | 6.507 | 3.67 | 2.065 | .698 | 1.376 |
| NADP | 5.343 | 32.2 | 1.903 | .564 | 1.341 |
| % DIFF | -19.6 | -13.0 | -8.1 | -21.2 | -2.5 |

References


Gran, G., 1952: Determination of the equivalence point in potentiometric titrations. Part 2, Analyst 77, 661-671.

Irving, P. M., 1978: Rainfall acidity at Argonne, Argonne National Laboratory Radiological and Environmental Research Division Annual Report, ANL-78-65, Part III, pp. 21-23.

Sisterson, D. L. and P. M. Irving, 1979: pH measurements of rain, Argonne National Laboratory Radiological and Environmental Research Division Annual Report, ANL-79-65, Part IV, pp. 61-64.

Sisterson, D. L., and G. T. Tisue, 1979: Comparison of the acidity of rain samples from ACM and PNL precipitation collectors, Argonne National Laboratory Radiological and Environmental Research Division Annual Report ANL-79-65, Part IV, pp. 65-67.

Sisterson, D. L., and D. Wagner, 1980: A comparison of the chemistry of event and weekly precipitation samples in northern Illinois -- A preliminary report, Part II, this report.

# A COMPARISON OF THE CHEMISTRY OF EVENT AND WEEKLY PRECIPITATION SAMPLES IN NORTHERN ILLINOIS -- A PRELIMINARY REPORT, PART 2

D. L. Sisterson and D. Wagner*

This preliminary report investigates the differences in chemical concentrations between weekly precipitation-weighted sums of event samples (ANL) and weekly (NADP) precipitation samples. Event samples are collected according to the Multistate Atmospheric Power Production Pollution Study (MAP3S) guidelines and weekly samples are collected because of membership in the National Atmospheric Deposition Program (NADP) network. The experimental procedure for the collection of precipitation is given in Part I of this report (see Sisterson and Wurfel, 1980).

Event samples were analyzed by liquid ion chromatography for $Na^+$, $K^+$, $NH_4^+$, $Cl^-$, $SO_4^=$, and $NO_3^-$, and by flame atomic absorption for $Ca^{++}$ and $Mg^{++}$ by the Analytical Chemistry Laboratory at Argonne. The samples were filtered with a 0.25 μm filter to remove debris during injection into the ion chromatograph and atomic absorption chamber. NADP samples were analyzed at the Central Analytical Laboratory at the Illinois State Water Survey in accordance with NADP guidelines with an autoanalyzer for all ions except $Ca^{++}$, $Mg^{++}$, $K^+$, and $Na^+$, whose concentrations were determined by flame atomic absorption.

Rain chemistry data for the 33-week study are presented for ANL and NADP precipitation samples in Table 1. Rigorous tests of statistical significance are in progress, but preliminary findings of the comparison of ANL and NADP data an summarized for the entire 33-week study period in Table 2. Generally, NADP samples contained more soil-derived material ($Ca^{++}$, $Mg^{++}$, and $K^+$), except for $K^+$. However, the ANL samples were apparently contaminated in some cases with small amounts of $K^+$, as an analysis of rinse water after bucket cleaning showed detectable amounts of $K^+$ (~ 0.05 mg/L) and NADP samples had $Cl^-$ values 10 to 30% higher than event samples. The $Na^+$ difference between ANL and NADP samples is unexpectedly large. Since NaCl from maritime tropical air masses is the primary source of $Na^+$ and $Cl^-$ in precipitation

* Student Aide (March - August 1981). Present affiliation: Northern Illinois University, Dekalb, Illinois.

Table 1. Chemical analysis of weekly summed event samples (ANL) and weekly samples (NADP) in mg/L.

| Sample | Date (1980) | $CA^{++}$ | | $Mg^{++}$ | | $K^{+}$ | | $Na^{+}$ | | $NH_4^{+}$ | | $NO_3^{-}$ | | $Cl^{-}$ | | $SO_4^{=}$ | |
|---|---|---|---|---|---|---|---|---|---|---|---|---|---|---|---|---|---|
| | | ANL | NADL | ANL | NADP | ANL | NADP | ANL | NADP | ANL | NADP | ANL | NADP | ANL | NADP | ANL | NADP |
| | | Milligrams/Liter | | | | | | | | | | | | | | | |
| 4 | 4/8 | .700 | .730 | .080 | .084 | .070 | .037 | .180 | .114 | .730 | .630 | 3.890 | 4.030 | .020 | .310 | 4.980 | 5.170 |
| 5 | 4/15 | | | | | | | CM | | | | | | | | | |
| 6 | 4/22 | | | | | | | NP | | | | | | | | | |
| 7 | 4/29 | | | | | | | CM | | | | | | | | | |
| 8 | 5/6 | | | | | | | NP | | | | | | | | | |
| 9 | 5/13 | -- | -- | .038 | .109 | .162 | .036 | .057 | 2.077 | .485 | .360 | 1.500 | 2.000 | -- | -- | 2.380 | 5.090 |
| 10 | 5/20 | .150 | .300 | .404 | .080 | .170 | .018 | -- | -- | .400 | .180 | 3.450 | 2.030 | -- | -- | 3.060 | 5.150 |
| 11 | 5/27 | | | | | | | IS | | | | | | | | | |
| 12 | 6/3 | .203 | .240 | .024 | .044 | .059 | .032 | .050 | .118 | .454 | .410 | 1.173 | 1.670 | .044 | .070 | 2.629 | 2.940 |
| 13 | 6/10 | .820 | .920 | .101 | .182 | .082 | .032 | .228 | .242 | .620 | .440 | 1.731 | 2.290 | .010 | .250 | 2.990 | 3.590 |
| 14 | 6/17 | .640 | .650 | .190 | .185 | .100 | .053 | .080 | .067 | .750 | .620 | 2.570 | 2.900 | -- | -- | 4.230 | 4.320 |
| 15 | 6/24 | .909 | 1.080 | .155 | .184 | .035 | .051 | .045 | .074 | 1.358 | 1.220 | .1985 | 3.320 | .123 | .220 | 5.017 | 5.050 |
| 16 | 7/1 | .640 | .730 | .180 | .193 | .090 | .046 | .080 | .345 | .730 | .420 | 2.260 | 2.530 | -- | -- | 6.270 | 6.700 |
| 17 | 7/8 | 2.830 | 2.860 | .730 | .570 | -- | -- | .440 | 6.245 | .110 | .580 | 5.000 | 5.101 | .560 | 1.020 | 7.890 | 14.260 |
| 18 | 7/15 | .360 | .440 | .060 | .088 | .050 | .052 | .070 | .102 | .240 | .160 | 1.310 | 1.710 | -- | -- | 2.480 | 2.880 |
| 19 | 7/22 | .659 | .690 | .076 | .117 | .079 | .029 | .092 | .047 | .676 | .530 | 2.464 | 2.370 | .044 | .230 | 5.475 | 5.420 |
| 20 | 7/29 | -- | -- | .170 | .075 | .097 | .026 | .055 | .152 | .739 | .670 | 2.410 | 3.880 | -- | -- | 6.755 | 6.450 |
| 21 | 8/5 | .714 | .800 | .142 | .155 | .150 | .084 | .121 | .113 | .581 | .410 | 2.313 | 2.350 | .023 | .220 | 4.116 | 4.190 |
| 22 | 8/12 | .360 | .370 | .050 | .060 | .090 | .050 | .160 | .070 | .720 | .520 | 2.930 | 3.100 | .060 | .220 | 4.290 | 4.400 |
| 23 | 8/19 | .290 | .360 | .060 | .080 | .340 | .290 | .290 | .120 | .620 | .310 | 2.190 | 2.250 | .140 | .310 | 4.870 | 4.600 |
| 24 | 8/26 | .250 | .190 | .404 | .040 | .060 | .020 | .070 | .130 | .460 | .250 | 1.580 | 1.730 | .260 | .280 | 3.810 | 3.840 |
| 25 | 9/2 | .180 | .140 | .030 | .020 | .606 | .010 | -- | -- | .330 | .270 | 1.300 | 1.370 | -- | -- | 2.970 | 3.310 |
| 26 | 9/9 | .220 | .230 | -- | -- | .090 | .020 | .130 | .030 | .730 | .510 | 1.750 | 1.940 | -- | -- | 2.260 | 2.430 |
| 27 | 9/16 | | | | | | | SC | | | | | | | | | |
| 28 | 9/23 | .040 | .210 | -- | -- | -- | -- | .101 | .030 | .200 | .210 | .510 | 1.170 | -- | -- | 1.030 | 1.630 |
| 29 | 9/30 | | | | | | | IS | | | | | | | | | |
| 30 | 10/7 | .660 | 1.400 | .190 | .517 | .190 | .111 | .200 | .132 | 1.180 | .580 | 1.290 | 2.220 | -- | -- | 1.240 | 2.530 |
| 31 | 10/14 | .820 | 1.050 | .050 | .328 | .050 | .081 | .060 | .062 | .460 | .390 | 1.570 | 1.560 | .100 | .150 | 3.080 | 3.690 |
| 32 | 10/21 | | | | | | | CM | | | | | | | | | |
| 33 | 10/28 | .130 | .220 | .040 | .058 | .050 | .021 | .020 | .033 | .490 | .280 | 1.340 | 1.250 | .100 | .200 | 2.460 | 3.330 |

CM, collector malfunction; NP, precipitation; IS, insufficient sample for analysis; SC, sample contamination.

Table 2. Chemical analysis of 33-week summed event (ANL) and weekly (NADP) precipitation samples. Percent difference is defined as the difference of the values (NADP-ANL) divided by the mean of the values.

| | $Ca^{++}$ | $Mg^{++}$ | $K^{+}$ | $Na^{+}$ | $NH_4^{+}$ | $NO_3^{-}$ | $Cl^{-}$ | $SO_4^{=}$ |
|---|---|---|---|---|---|---|---|---|
| ANL | 16.41 | 4.97 | 2.38 | 3.95 | 29.65 | 30.16 | 1.19 | 70.37 |
| NADP | 18.85 | 6.22 | 1.26 | 9.29 | 21.50 | 34.76 | 5.46 | 79.62 |
| % DIFF | 13.9 | 22.2 | -61.4 | 80.8 | -31.9 | 14.18 | 128.6 | 9.5 |

samples collected at Argonne, $Cl^{-}$ differences between ANL and NADP samples would not be expected to be significant. The greatest difference between ANL and NADP samples was in amounts of $NH_4^{+}$, $SO_4^{=}$, and $NO_3^{-}$. The NADP samples had less $NH_4^{+}$, but more $NO_3^{-}$ and $SO_4^{=}$.

It is hypothesized that the soil-derived material initially visible in the precipitation samples may slowly dissolve in the NADP samples. This is in agreement with the findings of Peden and Skowran (1978). Also, $CaCO_3$ and $MgCO_3$, which are found in abundance in northern Illinois, can react with the $H_2SO_4$ and $HNO_3$ in the precipitation and partially neutralize those acids. The differences in the concentrations of $NO_3^{-}$ and $NH_4^{+}$ may be explained by biological activity, particularly during the warm summer months. The difference in the concentration of $SO_4^{=}$, a stable compound, between ANL and NADP is currently under investigation.

## References


Peden, M. and L. Skowron, 1978: Ionic stability of precipitation samples. Atmos. Environ. 12, 2343-2349.

Sisterson, D. L. and B. E. Wurfel, 1980: A comparison of the acidity of event and weekly precipitation samples in northern Illinois -- A preliminary report, Part I, this report.

# ON THE SLOPE OF GRAN'S FUNCTION AS A CHECK FOR WEAK ACIDS IN PRECIPITATION

B. Wurfel,* B. Spencer,† and D. L. Sisterson

---

In most field studies of precipitation chemistry, pH electrode measurements of precipitation acidity are used to determine the amount of hydrogen ion deposition. However, the error in hydrogen ion concentration measured by pH electrodes at low ionic strength may be as large as 50% (Galloway et al., 1979). Alternatively, acidity can be determined by titrating precipitation samples with a standardized base according to Gran's method (1952). To determine whether there are dissociated weak acids present, samples can be further analyzed by back-titration with sulfuric acid to pH 3.0 after neutralization with sodium hydroxide to pH 5.0 (Irving et al., 1979). This report presents a method to determine the presence of dissociated weak acids with only the Gran method titration curve and the molarity of the base used. This should indicate when the time-consuming back-titration is necessary.

The concentration of the strong acid component is determined at ANL with Gran's function ( $\Psi$ ):

$$\Psi = (V_s + V_i)\ 10^{-pHi} \quad , \qquad (1)$$

where $V_s$ is the volume of the sample, $V_i$ is the volume of the base added, and $pH_i$ is the pH with successive additions of $V_i$. In order to obtain the strong acid concentration, $\Psi$ is plotted against $V_i$. Extrapolation of the relevant linear part of the Gran's function plot to the x-intercept indicates the amount of base needed to neutralize the strong acids. It has been shown that the absolute value of the slope of this line will equal the molarity of the base when weak acids are absent (Wurfel, 1981). The capability to detect a deviation from the molarity of the base in the slope due to the presence of weak acids has been investigated through simulation over a representative range of strong and weak acid concentrations and dissociation constants.

---

* Student Aide (May-August, December 1980). Present affiliation, Beloit College, Beloit, Wisconsin.

† Professor of Chemistry, Beloit College, Beloit, Wisconsin.

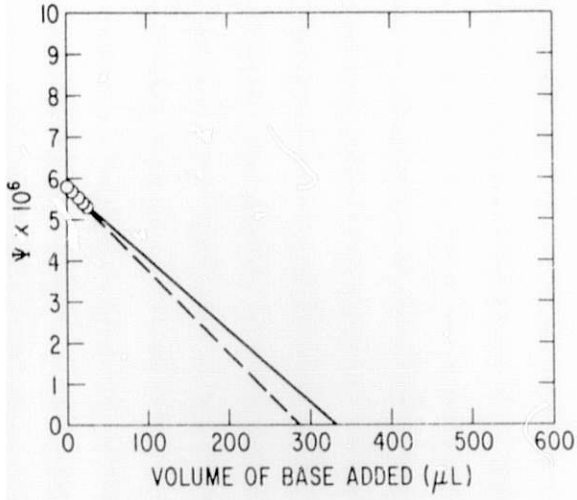


FIG. 1. Difference in equivalence points between solutions of strong acid (SA, 1 x $10^{-4}$ eq. $L^{-1}$, dashed line) and of both weak (WA, 2 x SA) and strong acids (solid line). Ka is the dissociation constant (1 x $10^{-5}$).

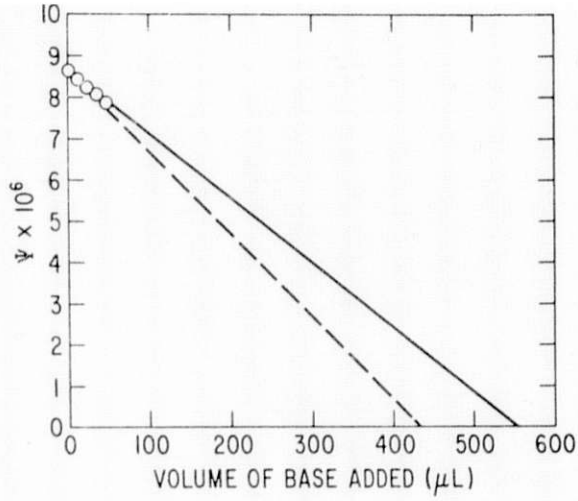


Figure 2. Difference in equivalence points between solutions of strong acid (SA, 1 x $10^{-4}$ eq. $L^{-1}$,) dashed line) and of both weak (WA, 2 x SA) and strong acids (solid line). Ka is the dissociation constant (1 x $10^{-4}$).

The equivalence points (x-intercept) for simulated titrations (Figure 1 of a solution containing hydrogen ions depend upon whether it is assumed that only strong acids are present or that both strong and weak acids are present. In both cases initial hydrogen ion concentration is the sam and the numerical value of the dissociation for the weak acid is ten times smaller than that of the hydrogen ion concentration. When the dissociation constant for the weak acid is equal to that of the hydrogen ion concentration, the deviation of the slope from the molarity of the base is the greatest (as in Figure 2); the difference in equivalent points is always even greater. However, it is difficult to measure weak acids that are an order of magnitude less than the strong acid concentration with current titration capabilities.

The data used to check the theory (Table 1) were collected at ANL (Sisterson and Wurfel, 1980). For this study, a difference between the slope and molarity of the base of less than 9 percent is considered indicative of the absence of weak acids. The methods agree in 17 of 24 samples tested. Only 3 of the back-titrated samples show the presence of dissociated weak acids. In these cases, the original titration curves indicate the presence of

Table 1. Analysis of rain samples for dissociated weak acids by the analysis of the slope of Gran's function and by the back titration method.

| | Presence of weak acids | |
|---|---|---|
| Rain sample | Analysis of Gran's slope | Back titration |
| Simulated rain | No | No |
| N/9 | No | No |
| M/9B | No | No |
| N/10 | No | No |
| M/10B | Yes | No |
| M/10C | No | No |
| N/12 | No | No |
| M/12A | No | No |
| M/12B | No | No |
| M/12C | No | No |
| M/12D | No | No |
| M/12E | No | No |
| N/13 | Yes | Yes |
| M/13B | Yes | Yes |
| M/13C | Yes | No |
| M/13D | Yes | Yes |
| N/14 | Yes | No |
| M/14A | No | No |
| N/15 | No | No |
| M/16A | Yes | No |
| N/17 | Yes | No |
| M/17A | No | No |
| N/18 | Yes | No |
| M/18A | Yes | No |

dissolved $CO_2$, which forms carbonic acid, a weak acid with a dissociation constant of $2.51 \times 10^{-6}$. However, the simple method indicates the presence of weak acids in 6 samples where the back-titration method indicates none. Thus, the back-titration method as employed at ANL may be less sensitive to the presence of dissociated weak acids.

Based on results to date, slope analysis from the original titration appears to provide at least a reliable screening procedure to decide whether back titration must be done, since the screening method identified every case where weak acids were present. Further work is being done to investigate the cases where the two methods disagreed.

References

Galloway, J. N., B. J. Cosby, Jr., and G. E. Likens, 1979: Acid precipitation: Measurement of pH and acidity, Limnol. Oceanogr. 24, 1161-1165.

Gran, G., 1952: Determination of the equivalence point in potentiometric titrations, Part 2, Analyst 77, 661-671.

Irving, P. M., D. L. Sisterson, and S. Mermall, 1979: Strong and weak acids in precipitation at Argonne, 1979, Argonne National Laboratory Radiological and Environmental Research Division Annual Report ANL-79-65, Part III, pp. 47-48.

Wurfel, B. E., 1981: Investigation of Gran's method on acid precipitation studies, Thirty-Second Annual Student Research Symposium, sponsored by the American Chemical Society, DePaul University, Chicago, Illinois, May 2, 1981.

Sisterson, D. L. and B. E. Wurfel, 1980: A comparison of the acidity of event and weekly precipitation samples in northern Illinois-A preliminary report, Part I, this report.

# THE OPEN-FRAME HEAT FLUX PLATE - A NEW DESIGN

D. R. Cook

Soil heat flux density measurements made with solid heat flux plates can contain significant errors as a consequence of the plate design. Most commercially-available solid plates are thermopiles embedded in a small ceramic disc or epoxy-resin lamination, sandwiched between stainless steel or anodized aluminum plates; most home-made solid devices are thermopiles wrapped around a glass microscope slide and then covered with epoxy for durability and waterproofing (Tanner, 1963; Cook, 1977). These designs result in a fixed thermal conductivity, rarely that of the soil, and restrict the movement of water and water vapor. Air and water gaps between the soil and the plate, in effect, alter the thermal conductivity of the plate. In addition, radiation errors may occur when the plate is placed too near (less than 5 cm) the soil surface. A new open-frame plate has been designed to eliminate or minimize these errors.

The open-frame design has a wooden framework around which thermopiles are wrapped and then waterproofed, as in Figure 1. The wooden framework is durable and yet thin enough that any obstruction to heat and water flow is minimal. This design has several attractive characteristics. Water and water vapor can move freely between the thermopile elements. The thermal conductivity of the plate is that of the soil in which it is implanted; therefore, calibration is necessary only over the likely range of temperature gradients encountered in the soil.

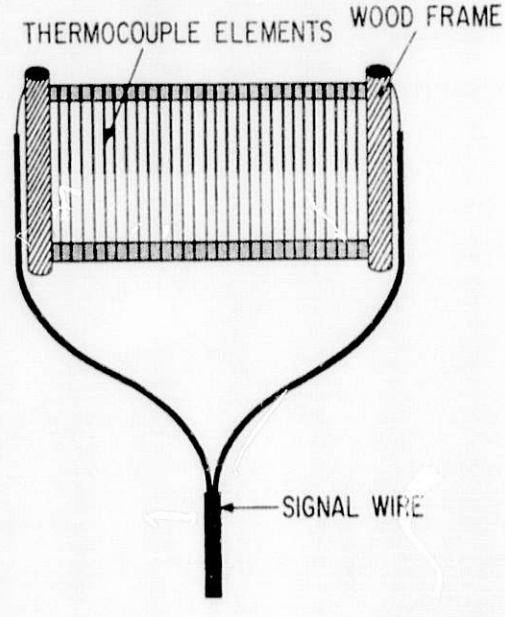


FIG. 1. Open-frame heat flux plate.

The thermal conductivity of the soil or snow must be monitored continously during use of the device. This can be accomplished with a thermal conductivity probe or with a calorimetric analysis of the soil, accompanied by soil moisture measurements made with a microlysimeter or soil water tensiometers. The latter device gives only a rough estimate of soil water content. The criteria of Philip (1961) for relative error measurement,

$$r = \frac{\text{plate thickness}}{\text{plate area}} < 0.1 \qquad (1)$$

is met by the open design:

$$r = \frac{3 \text{ mm}}{46 \text{ mm} \times 88 \text{ mm}} = 0.047 \qquad (2)$$

The only air and water gaps that can occur are between individual thermopile elements and the soil. Nevertheless, significant errors could result from too many such gaps. The small cross-sectional area of the open plate (which is essentially the cross-sectional area of the thermopile elements) minimizes radiation errors and therefore, permits it to be placed within 1 cm of the soil surface. Since heat flux plate sensitivity increases with increasing soil temperature gradient, it is advantageous to place the device near the surface, where the temperature gradient is greatest.

The open design can be used in snow as well, since water that melts and leaches down through the snow will pass through the device and not form a water or ice gap between the snow and the plate. This has been demonstrated with a prototype. The wood frame should be painted white to reduce absorption of solar radiation.

Since the open design has approximately one-half the number of thermopile elements of a soild plate, the voltage output is expected to be about half that of a solid plate. This is not a significant problem except in cases of very small fluxes. The most restrictive disadvantage of the open design is its lack of durability; freezing-thawing cycles or compaction of the soil or snow could cause the thermopile elements to break. This problem could be partially remedied by using thermopile wire of larger diameter than in the current design. Calibration and testing of the open-frame design in both snow and soil will be pursued during the next year to determine performance and potential.

References

Cook, D. R., 1977: The effect of combined soil warming and irrigation on the soil surface energy budget, M.S. Thesis, The Pennsylvania State University.

Philip, J. R., 1961: The theory of heat flux meters, J. Geophys. Res. 66, 571-579.

Tanner, C. B., 1963: Soils Bulletin 6; Basic Instrumentation and Measurements for Plant Environment and Micrometeorology, Dept. of Soil Science, Univerity of Wisconsin.

# WASTE HEAT UTILIZATION BY SOIL WARMING

D. R. Cook

---

The electrical power produced by turbines typically accounts for only one-third of the total energy produced by fuel combustion; the other two-thirds is manifested in the thermal energy of turbine cooling water. Electricity generating plants often use a small amount of thermal energy to heat plant buildings, but most of the heat is dissipated to the environment, with no economic gain. About a decade ago a system was conceived to utilize much of this waste heat. The concept grew out of work that showed potentially significant benefits to agriculture as a result of soil warming by artificial means (Boersma et al., 1972). The essence of the proposed system, later simulated with a small-scale prototype (Dewalle, 1974; 1978), was that waste hot water would be pumped through buried pipes. The experimental data generated were used with an advection model to determine the heat dissipation ability of a full-scale buried-pipe system serving a 1500 MW electricity generating plant (Cook and Norman, 1981).

The experimental system consisted of a 15 × 60 m buried-pipe prototype and an adjacent 15 × 30 m unheated control plot located in a field in central Pennsylvania. The water temperature in the 5 cm diameter prototype pipes was strictly maintained at 311° K by a thermostatically-controlled heating system in order to simulate generating plant waste hot water. The flow-rate (3.4 cm $s^{-1}$) through the pipes, however, was smaller by a factor of twenty than that of a full-scale system. This was necessary for practical reasons, such as pump size and heating system expense. Corrections for this difference were applied to the advection model results. From Reynolds number studies performed on the prototype, it was estimated that heat dissipation would be doubled if the greater flow-rate were used.

The prototype and control were regularly irrigated with secondary-treated sewage effluent to increase soil thermal conductivity and thereby increase heat dissipation. Nutrient-rich effluent was chosen to increase productivity and reduce irrigation costs.

Tables 1 and 2 present the results of the study in terms of the average heat dissipation rate and the land area required for heat dissipation

Table 1. Annual average heat dissipation.

| | Dissipation rate, $Wm^{-2}$ | Land area required ha |
|---|---|---|
| Prototype | 78 | 5597 |
| Advection model results | 54 | 8085 |
| Corrected for full-scale flow rate | 111 | 3933 |

Table 2. Seasonal average heat dissipation.

| | Dissipation rate, $Wm^{-2}$ | | Land area required ha | |
|---|---|---|---|---|
| | Summer | Winter | Summer | Winter |
| Prototype | 45 | 109 | 9686 | 4011 |
| Advection model results | 30 | 77 | 14685 | 5708 |
| Corrected for full-scale flow rate | 63 | 158 | 6924 | 2772 |

for a typical 1500 MW electricity generating plant (4366 MW thermal power at 34.4% efficiency). The enhanced sensible and latent heat fluxes from the soil produce an insignificant effect on those qualities at the downwind edge of the small plot. However, advection over the length of the full-scale system reduces the dissipation ability of the system. Table 2 shows that seasonal considerations favor the use of a buried-pipe system in the winter, when the air-to-ground temperature difference is greatest. Altogether, the results are not as encouraging as those obtained by a previous, similar study (Skaggs et al., 1973). However, the prototypes were smaller, and no modeling to full-scale was attempted in that study.

Engineering cost-efficiency studies by Plummer (in Dewalle, 1974) suggest that a land area of 1821 ha is the economically optimum size for a buried-pipe system serving a 1500 MW electricity generating plant. These studies do not claim that this size system can dissipate all of the waste heat generated by such a plant. A larger system would not be competitive with conventional cooling systems in that it would require a capital outlay greater than could be recovered in benefits to agriculture during the expected life span of an electricity generating plant. The 1821 ha is less than half that needed to dissipate all of the waste heat from a 1500 MW plant, on an annual average. Such a system could be employed practicably only as a system supplementary to conventional cooling methods. Even so, the agricultural and environmental benefits could be great in cool climates. Expansion of the buried-pipe land area to increase power plant efficiency, and thereby reduce fuel costs, may be cost-efficient in the future. However, fuel prices would have to rise than land values before soil warming could begin to be cost competitive with conventional cooling methods.

## References


Boersma, L., E. Barlow and K. Rykbost, 1972: Use of reactor cooling water from nuclear power plants for irrigation of agricultural crops, Water Resources Research Institute, Oregon State University, WRRI-12.

Cook, D. R., and J. M. Norman, 1981: Soil warming as an alternative to conventional waste heat dissipation, submitted for publication.

Dewalle, D. R., Ed., 1974: An agro-power-waste-water complex for land disposal of waste heat and waste water, Pennsylvania State University, Institute for Research on Land and Water Resources, Res. Publ. 86.

Dewalle, D. R., ed., 1978: Soil-warming for waste heat disposal, crop growth enhancement and waste water renovation, Pennsylvania State University, Institute for Research on Land and Water Resources, National Technical Information Service, Springfield, VA., Report PB-290902.

Skaggs, R. W., C. R. Willey, and D. C. Sanders, 1973: Use of waste heat for soil warming in North Carolina. ASSE, 1973 Winter meeting, Chicago, Illinois, Dec. 11-14, Paper No. 73-3530.

Williams, G. G., 1972: TVA-programs-waste utilization in greenhouses and other agriculturally related projects, Proc. National Conference Waste Heat Utilization, M. Yarosh, Ed., Oak Ridge National Laboratory,

PUBLICATIONS BY THE STAFF OF THE ATMOSPHERIC PHYSICS SECTION FOR THE PERIOD JANUARY-DECEMBER 1980

## Journal Articles, Book Chapters, etc.

R. L. Coulter and M. L. Wesely
ESTIMATES OF SURFACE HEAT FLUX FROM SODAR AND LASER SCINTILLATION MEASUREMENTS IN THE UNSTABLE BOUNDARY LAYER
J. Applied Meteorol. 19(10), 1209-1222 (October 1980)

R. L. Coulter and K. H. Underwood
SOME TURBULENCE AND DIFFUSION PARAMETER ESTIMATES WITHIN COOLING TOWER PLUMES DERIVED FROM SODAR DATA
J. Applied Meteorol., 19(12), 1395-1404, (December 1980)

B. B. Hicks
INVESTIGATIONS OF SPARGING AS A METHOD FOR PROMOTING COOLING POND HEAT TRANSFER
J. Applied Meteorol. 19, 193-198 (February 1980)

B. B. Hicks, M. L. Wesely, and J. L. Durham
CRITIQUE OF METHODS TO MEASURE DRY DEPOSITION, WORKSHOP SUMMARY
Final Report to Environmental Sciences Research Laboratory, EPA, RTP. EPA-600/9-80-050. (1980). NTIS PB81-126443.

C. M. Sheih
PASQUILL-TAYLOR DISPERSION PARAMETERS OVER WATER NEAR SHORE
Atmos. Environ., 15, 101-105 (April 1980)

C. M. Sheih, P. Frenzen, and R. L. Hart
MEASUREMENTS OF LAGRANGIAN ATMOSPHERIC DISPERSION STATISTICS OVER OPEN WATER
J. Applied Meteorol., 19(4), 497-504 (May 1980)

C. M. Sheih
ON LATERAL DISPERSION COEFFICIENTS AS FUNCTIONS OF AVERAGING TIME
J. Applied Meteorol., 19, 557-561 (May 1980)

M. L. Wesely
COMMENTS ON "BULK PARAMETERIZATION OF AIR-SEA EXCHANGES OF HEAT AND WATER VAPOR INCLUDING THE MOLECULAR CONSTRAINTS AT THE INTERFACE
J. Atmos. Sci. 37(12), 2797-2800 (December 1980)

## Conference Papers and Abstracts

B. B. Hicks
ON THE DRY DEPOSITION OF ACID PARTICLES TO NATURAL SURFACES
Proceedings of the 12th Rochester International Conference on Environmental Toxicity: Polluted Rain, held in Rochester, NY, May 21-23, 1979 (April 1980)

B. B. Hicks and M. L. Wesely
TURBULENT TRANSFER PROCESSES TO A SURFACE AND INTERACTION WITH VEGETATION
Proceedings of the Second Life Sciences Symposium, Gatlinburg, TN, October 14-18, 1979. Atmospheric Sulfur Deposition, Environmental Impact and Health Effects (eds. D. S. Shriner, C. R. Richmond, and S. E. Lindberg). Ann Arbor Publishers Inc. (1980).

J. D. Shannon
EXAMINATION OF SURFACE REMOVAL AND HORIZONTAL TRANSPORT OF ATMOSPHERIC SULFUR ON A REGIONAL SCALE
Reprint: Conference on Applications of Air Pollution Meteorology and Second Conference on Industrial Meteorology, March 24-28, 1980, New Orleans, LA, 232-235 (1980)

M. L. Wesely
COMPARISONS OF SURFACE-RENEWAL PREDICTIONS WITH FIELD DATA
Preprint: Winter Annual Meeting, Nov. 16-21, 1980, Chicago, Ill., ASME, 80-WA/HT-67.

T. Yamada
NUMERICAL SIMULATION OF MESOSCALE ATMOSPHERIC CIRCULATIONS OVER THE LAKE MICHIGAN
Winter Annual Meeting, The American Society of Mechanical Engineers, 80-WA/HT-65 (November 1980).

T. Yamada
AIR CIRCULATIONS OVER A GAUSSIAN-SHAPED VALLEY
Second Joint Conference on Applications of Air Pollution Meteorology and Second Conference on Industrial Meteorology, New Orleans, La., The American Meteorological Society, 505-509 (March 1980).